Synthesis Of Alkylthiol-containing Fluorene Derivatives For Gold Nanoparticle Functionalization

Sriram Mukundarajan
University of Central Florida

University of Central Florida

STARS
Showcase of Text, Archives, Research & Scholarship

SYNTHESIS OF ALKYLTHIOL-CONTAINING FLUORENE DERIVATIVES FOR
GOLD NANOPARTICLE FUNCTIONALIZATION.

by

SRIRAM MUKUNDARAJAN
B.S. University of Madras, 2001

A thesis submitted in partial fulfillment of the requirements
for the degree of Master of Science
in the Department of Chemistry
in the College of Arts and Sciences
at the University of Central Florida
Orlando, Florida

Fall Term
2005

ABSTRACT

A novel synthetic methodology has been developed for attaching fluorene derivatives, containing different types of electron donating and accepting groups at the 2 and 7 positions, to gold nanoparticles of different sizes by exploiting the affinity of the thiol functional group for gold. The distance between the dye and nanoparticles was varied by introducing two alkyl chains containing different number of carbon atoms at the 9 position on the fluorene ring system. The methodology that was developed gave enough scope for performing Radiative Decay Engineering (RDE) studies, in order to investigate the impact of gold nanoparticles on the singlet oxygen quantum yields of fluorene dyes that already exhibit high singlet oxygen quantum yields as well as high two photon absorption (2PA) cross-sections.

The dialkylation of the fluorene derivatives was accomplished by reacting the dye with α, ω-dibromoalkanes containing different number of carbon atoms in a biphasic reaction mixture containing toluene and aqueous sodium hydroxide solution in the presence of tetrabutylammonium bromide (TBAB) as a phase transfer catalyst. The bromine atom on the alkyl chains was converted to thioester by reaction with potassium thioacetate. This was followed by the hydrolysis of the thioester to form the thiol moiety. The compounds synthesized were characterized using ^{1}H and ^{13}C nuclear magnetic resonance (NMR) spectroscopy and elemental analysis.

Functionalization of gold nanoparticles was attempted by bringing into contact a solution of the thiol compound in toluene and an aqueous gold nanoparticles solution. UV-vis absorbance spectroscopy was used to monitor the progress of the attachment.

Surface Enhanced Raman Scattering (SERS) spectroscopy was used to probe the

enhancement of Raman signal by the metallic nanoparticles.

To my parents, Mrs. Bhama Mukundarajan and Mr. K.E. Mukundarajan

ACKNOWLEDGMENTS

I would like to first of all acknowledge the vision and mentorship of Dr. Kevin D. Belfield, whose ideas made this work possible. It is the greatest honor to be a part of his research group.

I am highly grateful to Dr. Florencio E. Hernandez for his constant support and encouragement throughout the course of this work. I would like to express my sincere gratitude to the Department of Chemistry for providing me financial assistance in the form of a teaching assistantship.

I acknowledge the assistance and camaraderie of all my fellow group members especially Dr. Sheng Yao, Dr. Katherine Schafer, Stephen Andrasik, Mohammed Daoudi and Li Zhang. I would like to express my deepest appreciation to Marisol Garcia for her help in synthesizing gold nanoparticles that were used in this study and Natarsha Davis for her help in formatting this document.

Finally, I extend my deepest gratitude to my parents, sister Renuka and brothers Venkat, Bharath for standing by me all through these years and believing in my potential for success.

TABLE OF CONTENTS

LIST OF FIGURES

LIST OF TABLES

LIST OF SCHEMES

LIST OF SYMBOLS AND ABBREVIATIONS

Γ radiative rate

Γ_m radiative rate in the presence of metal

k_{nr} non radiative decay rate

τ_0 lifetime of fluorophore in the absence of metal

τ_N natural lifetime of fluorophore

Φ_Δ singlet oxygen quantum yield

k_q rate constant for collisional quenching

2PA   Two Photon Absorption

AcOH   acetic acid

ANS   8-Anilino-1-naphthalenesulfonic acid

Au-MPCs   Monolayer Protected Gold Clusters

$CDCl_3$ deuterated chloroform

d   doublet

KOAc   potassium acetate

m   multiplet

MPC   Monolayer Protected Clusters

NIR   Near Infrared

NMR   nuclear magnetic resonance

PDT   Photodynamic Cancer Therapy

ppm   parts per million

PS   Photosensitizer

Q_m quantum yield of fluorophore in the presence of metal

Q_0	quantum yield of fluorophore in the absence of metal
Q_u	quencher concentration
RBF	Round Bottom Flask
RDE	Radiative Decay Engineering
RET	Resonance Energy Transfer
SERS	Surface Enhanced Raman Scattering
SPR	Surface Plasmon Resonance
t	triplet
TBAB	tetrabutylammonium bromide
TLC	Thin Layer Chromatography

CHAPTER ONE: INTRODUCTION

1.1 Radiative Decay Engineering

The term Radiative Decay Engineering (RDE) refers to the process by which the emission of fluorophores or chromophores can be modified by increasing or decreasing their radiative decay rates (fluorescence)[1]. Over the past decade, fluorescence spectroscopy has gained a lot of prominence in the field of biochemistry and molecular biology. Fluorescence has also become the dominant method enabling the revolution in medical diagnostics[2], DNA sequencing[3] and genomics[4]. Most of these applications involve use of fluorescence observables such as spectral shifts, anisotropies, quantum yields and lifetimes. RDE provides a new scope for enhancing the applications of fluorescence spectroscopy.

In most fluorescence experiments the radiative rates are not changed because these rates depend on the extinction coefficient of the fluorophore. This intrinsic rate is not changed by quenching and is only weakly dependent on environmental effects. Spectral changes are usually caused by changes in the non radiative rates resulting from quenching or resonance energy transfer. These processes affect the emission by providing additional routes for decay of the excited states without emission. In contrast to the relatively constant radiative rates in free solution, it is known that the radiative rates can be modified by placing the fluorophores at suitable distances from the metallic surfaces and particles[5-8].

Depending upon the distance and geometry, metal surfaces or particles can result in quenching of fluorescence or enhancement of fluorescence by factors of up to 1000[9-11]. The effect of metallic surfaces on fluorophores is at least due to three mechanisms. One is

1

energy transfer quenching to these metals with a d^3 dependence[9], where d is the distance between the fluorophore and the metal. The quenching can be understood by damping of the dipole oscillators by the nearby metal. A second mechanism is an increase in intensity due to the metal amplifying the incident field, which has been seen for metal colloids[11-13]. The enhancement can be understood as due to the metal particles on concentrating the local excitation intensity. These effects of quenching and enhancing the local fields are important.

However another more important effect of metal surfaces and particles is possible. This effect is that the nearby metal can increase the intrinsic decay rate of the fluorophore[1]. This is a highly unusual effect. In fluorescence spectroscopy, there is no significant control over the radiative rate (Γ). The spectral observables of quantum yields and lifetimes are governed by the magnitudes of the radiative rate Γ and the sum of the nonradiative decay rates (k_{nr}). To understand the value of controlling the radiative decay rate (Γ), it is informative to consider how this rate affects the quantum yield Q_0 and lifetime τ_0 of a fluorophore in the absence of a metal surface. Consider the Jablonski diagram in Figure 1.
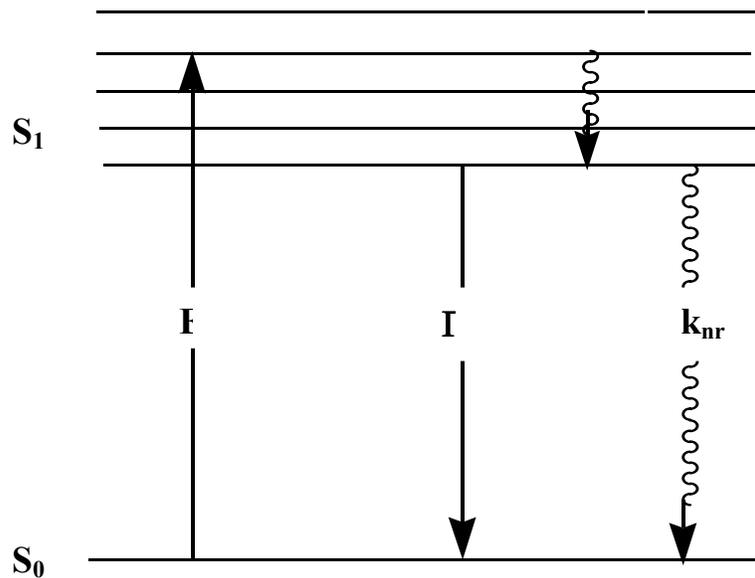
Figure 1. Simplified Jablonski diagram

The quantum yield Q_0, is the fraction of the excited fluorophores which decay by emission (Γ) relative to the total decay ($\Gamma + k_{nr}$). The quantum yield of the fluorophore in the absence of other quenching interactions is given by

$$Q_0 = \Gamma/(\Gamma + k_{nr})$$

The radiative rate is determined by the oscillator strength (extinction coefficient) of the electronic transition. The extinction coefficients of chromophores are only slightly dependent on their environment. Hence, the quantum yield can only be increased by decreasing the nonradiative rate k_{nr}, which usually occurs at lower temperatures.

Fluorophores with high radiative rates have high quantum yields and short lifetimes. The lifetime of a fluorophore is determined by the sum of the rates which depopulate the excited state. In the absence of other quenching interactions the lifetime is given by

$$\tau_0 = (\Gamma + k_{nr})^{-1}$$

3

The lifetime of a fluorophore can be increased or decreased by changing the value of k_{nr}. The natural lifetime of a fluorophore (τ_N) is the inverse of the radiative decay rate ($\tau_N = \Gamma^{-1}$) or the lifetime which would be observed in the absence of any sort of nonradiative decay ($k_{nr} = 0$). Almost invariably, the lifetimes and quantum yields increase or decrease together. Most fluorescence experiments involve changing the rates of nonradiative decay. For instance, collisional quenching with a biomolecular rate constant k_q decreases the quantum yield and lifetime according to

$$Q = \Gamma/(\Gamma + k_{nr} + k_q[Q_u]),$$

where $[Q_u]$ is the quencher concentration. The lifetime of the quenched fluorophore is decreased by the additional nonradiative path to the ground state with a rate $k_q[Q_u]$

$$\tau = (\Gamma + k_{nr} + k_q[Q_u])^{-1}.$$

Similarly, resonance energy transfer (RET) results in an additional rate process which depopulates the excited state.

$$k_T = (1/\tau_0)(R_0/r)^6$$

The decay time in the presence of energy transfer is given by

$$\tau = (\Gamma + k_{nr} + k_T)^{-1}$$

Both quenching and RET decrease the quantum yield and lifetime of the fluorophore. The radiative rate Γ, is not changed by these processes.

The absolute and relative brightness of a fluorophore are dependent on the values of the radiative and non-radiative decay rates. For instance, the radiative decay rates of the nucleic acid bases are comparable to those of typical fluorescent probes. However, the emission is very weak ($Q_0 < 10^{-4}$) and the lifetimes very short (approx 10ps) because of the high rates of nonradiative decay (approx $10^{11} s^{-1}$)[14]. In general there

is no way to control the lifetime or quantum yield of a fluorophore other than altering the values of k_{nr}, $k_q[Q_u]$, or k_T.

This is where the term "Radiative Decay Engineering" assumes its significance. It is informative to consider the novel spectral effects expected by increasing the radiative rate by Γ_m due to the addition of a metal surface (Figure 2)[1]. For the present discussion the quenching effects of the metal (k_m) are neglected. In this case the quantum yield (Q_m) and lifetime (τ_m) of the fluorophore near the metal surface are given by

$$Q_m = (\Gamma + \Gamma_m) / (\Gamma + \Gamma_m + k_{nr})$$

$$\tau_m = (\Gamma + \Gamma_m + k_{nr})^{-1}.$$
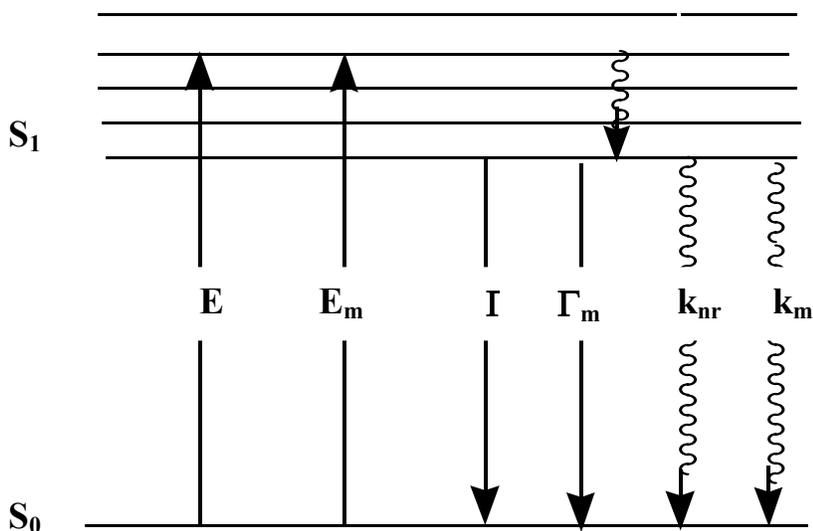
Figure 2. Simplified Jablonski diagram in the presence of a metal

These equations result in unusual predictions for a fluorophore near a metal surface. As the value of Γ_m increases, the quantum yield increases while the lifetime decreases. This was proven by the calculation of the lifetime and quantum yield for fluorophores with an assumed natural lifetime $\tau_N = 10ns$, $\Gamma = 10^8 s^{-1}$ and various values for

the nonradiative decay rates and quantum yields. The values of k_{nr} varied from 0 to 9.9 x

$10^7 s^{-1}$, resulting in quantum yields from 1.0 to 0.01.
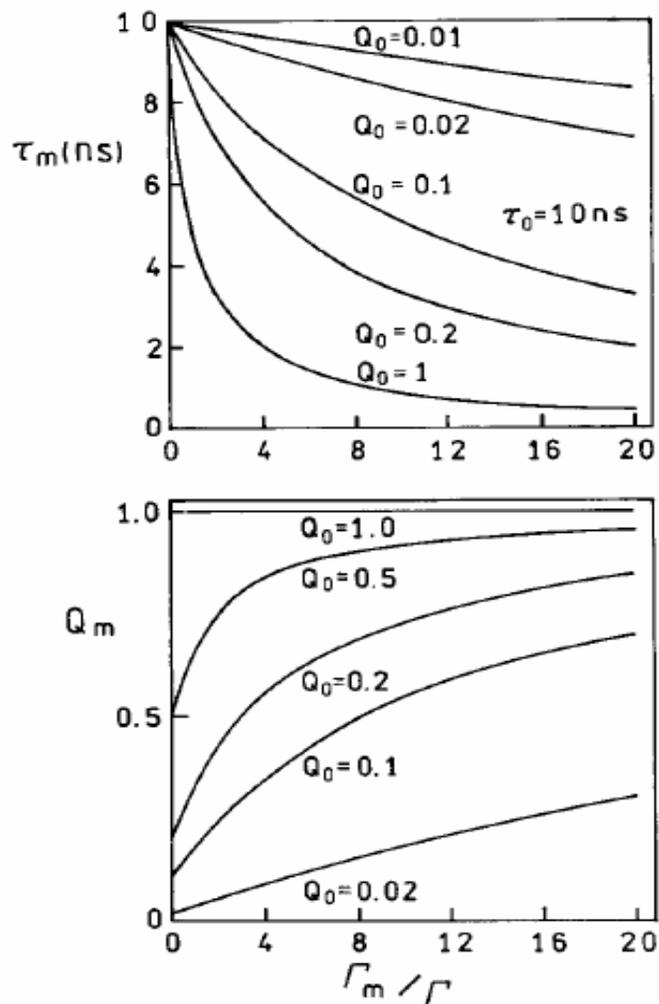
Figure 3. Effects of an increase in the metal induced radiative rate on the lifetime and quantum yields of fluorophores.[1]

As expected, the lifetime decreases as Γ_m becomes comparable and larger than Γ (Figure 3). This is a typical result, similar to that which occurs for increasing amounts of collisional quenching. However, an unusual effect is expected for the quantum yield. As Γ_m increases, the quantum yield increases. The most dramatic relative changes are found for fluorophores with the lowest quantum yields. If $Q_0 = 1.0$, then changing Γ_m has no effect. If Q_0 is low, such as 0.1 the metal induced rate Γ_m increases the quantum yield. At sufficiently high values of Γ_m, the quantum yields of all fluorophores approach 1.0. Examination of figure 3 reveals that larger values of Γ_m/Γ, are required to change the lifetime or quantum yield of low quantum yield fluorophores. This effect occurs because, for the same unquenched lifetime τ_0, lower quantum yields imply larger values of k_{nr}. Larger values of Γ_m are required to compete with the larger values of k_{nr}.
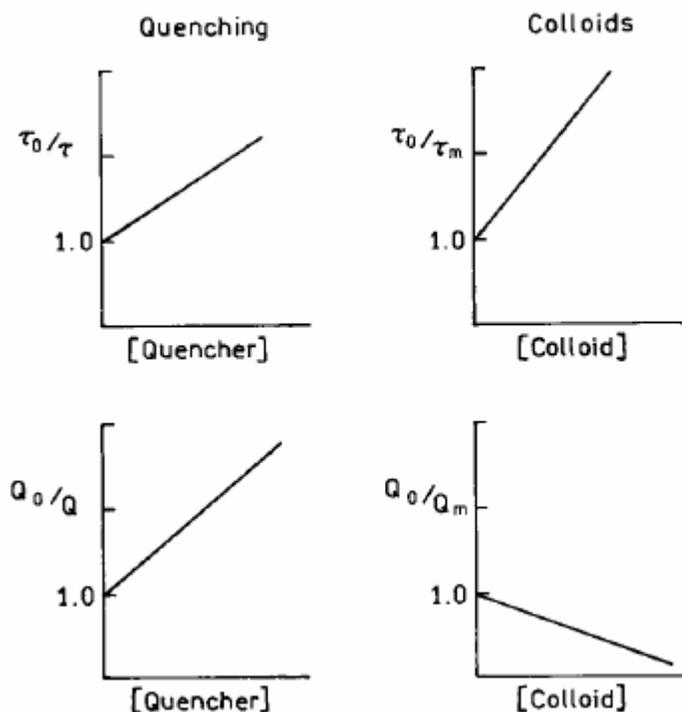
Figure 4. Comparison of Stern-Volmer plots for collisional quenching and colloids which enhance Γ_m.[1]

It is informative to compare the effects of increasing values of Γ_m with increasing amounts of quenching. Figure 4 shows this comparison in terms of the Stern-Volmer plots. The effects of the rate Γ_m are dramatically different from the effects of the rate-collisional quenching $k_q[Q_u]$. In the case of collisional quenching both the lifetimes and quantum yields decrease (Figure 4). The effects of metallic colloids which increase Γ_m are dramatically different. In this case the lifetimes decrease but the quantum yields increase.

The increases in quantum yields which can occur near metal surfaces are different from the typical increase in quantum yield which occurs when a solvent-sensitive fluorophore like 8-Anilino-1-naphthalenesulfonic acid (ANS) is dissolved in a low polarity solvent or binds to a protein[15-16]. In these cases the quantum yield increases because of a decrease in the nonradiative decay rate k_{nr}.

8

1.2 Metallic Surface Effects on Fluorescence

The possibility of altering the radiative decay rates was demonstrated by measurements of the decay times of an europium (Eu^{3+}) complex positioned at various distances from the planar silver mirror (Figure 5)[5-8].
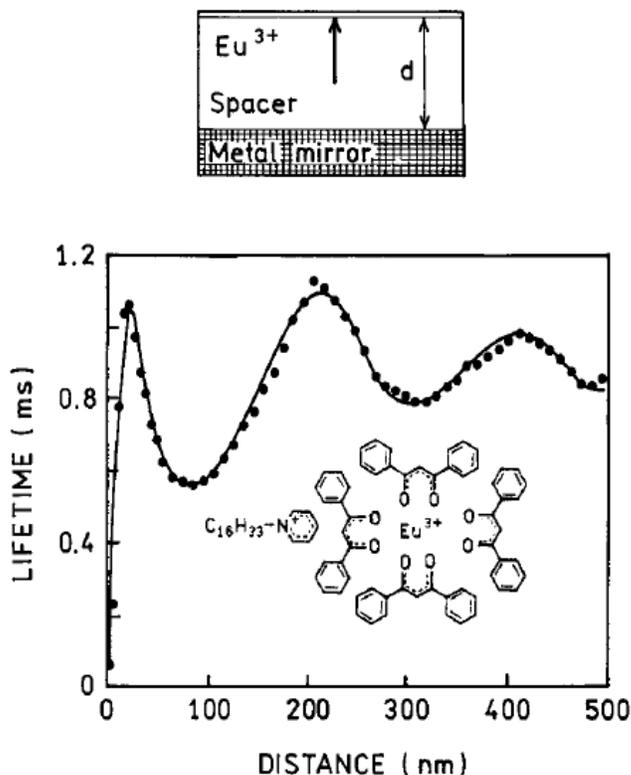
Figure 5. Lifetime of Eu3+ ions in front of a Ag mirror as a function of separation between the Eu3+ ions and the mirror. The solid curve is a theoretical fit.

In a mirror the metal layer is thicker than the optical wavelength. The lifetimes oscillate with distance but remain a single exponential at each distance. This effect can be explained by changes in the phase of the reflected field with distance and the effects of this reflected field on the fluorophore. A decrease in lifetime is found when the reflected field is in phase with the fluorophore's oscillating dipole. An increase in the lifetime is found if the reflected field is out of phase with the oscillating dipole. As the distance

increases, the amplitude of the oscillations decreases. The effects of a plane mirror occur over distances comparable to the excitation and emission wavelengths. At short distances below 20nm the emission is quenched. This effect is due to coupling of the dipole to oscillating surface changes on the surface of the metal, which are called surface plasmons resonances (SPR).

The effects of metallic surfaces on optical spectra are strongly dependent on the nature of the metal surface and /or metal particles. In most cases more dramatic effects are observed for metal colloids than planar mirrored surfaces. For example, Raman signals are remarkably enhanced by metal colloids or islands[17, 18], which has resulted in the field of Surface Enhanced Raman Scattering (SERS).

1.3 Surface Plasmon Effect

Metal colloids have been used for centuries to make colored glasses[19]. Typical absorption spectra of gold colloids are shown in figure 6[20].
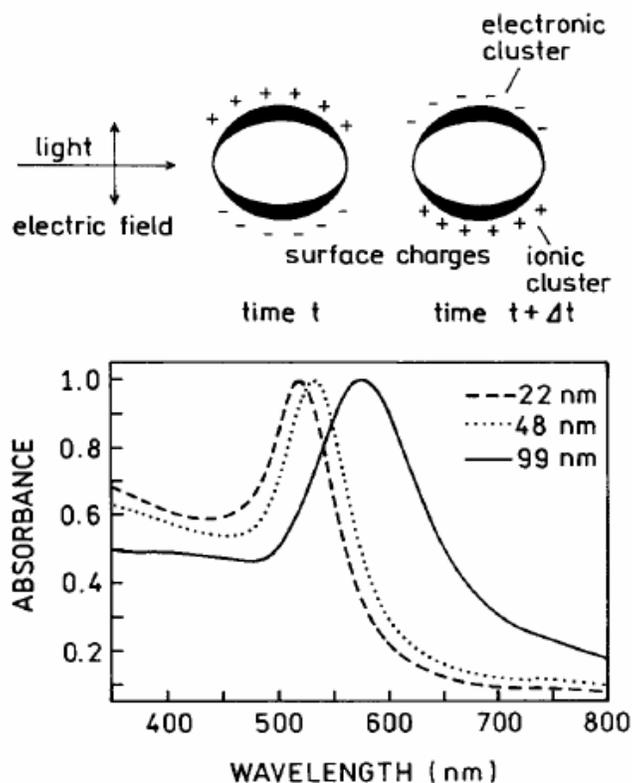
Figure 6. Absorption spectra of gold colloidal spheres

The long wavelength absorption is called the surface plasmon absorption, which is due to electron oscillations on the metal surface. These spectra can be calculated for the small particle limit (r « λ) from the complex dielectric constant of the metal[21]. Larger particles display longer wavelength absorption (Figure 6).There are several interactions between fluorophores and metallic surfaces[22-25].

These effects are shown schematically in Figure 7 which include quenching, enhancement of the strength of the incident light field and an increase in the radiative decay rate of the fluorophore.

11
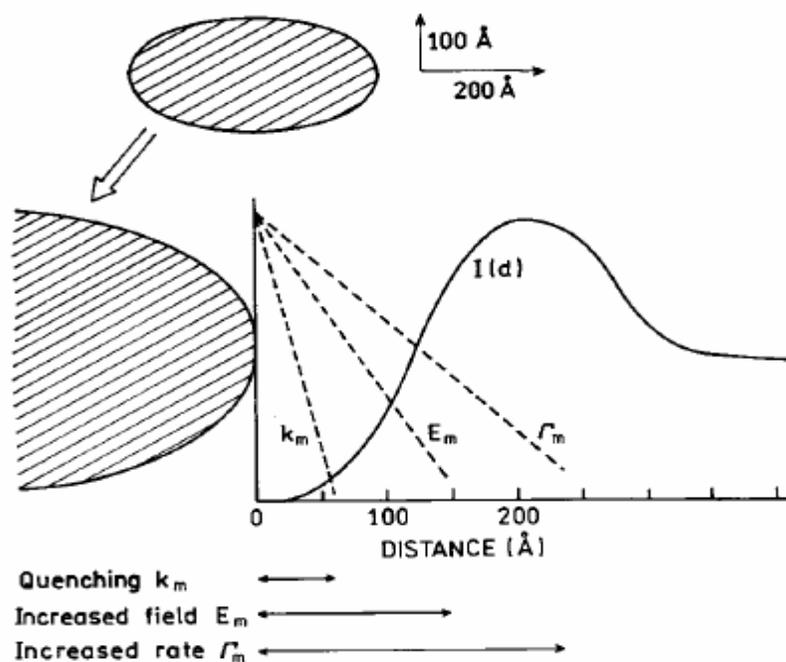
Figure 7. Effects of a metallic particle on transitions of a fluorophore. Metallic particles can cause quenching (knr), can concentrate the incident light field (Em), and can increase the radiative decay rate (Γm).1

Quenching occurs by Forster transfer to the surface plasmon absorption of the metal. This effect decreases with the cube of the distance (d) between the metal surface and the fluorophore (d^{-3})[9].

The metal particles are known to concentrate the local field of incident light. This effect has been modeled for ellipsoidal particles and the maximum enhancement in the magnitude of the local field is about 140[23]. Since the light intensity is proportional to the square of the field, metal particles can result in greatly enhanced local excitation intensities.

The presence of a metallic particle can have dramatic effects on the radiative decay rate of a nearby fluorophore. Several groups have considered the effects of metallic spheroids on the spectral properties of nearby fluorophores.[22-25]

12
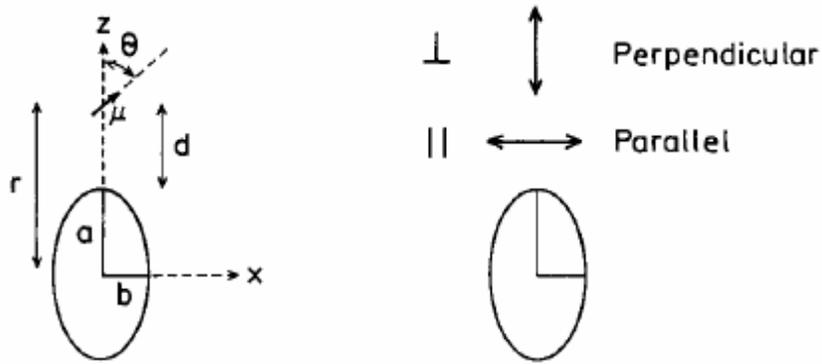
Figure 8. Fluorophore near a metallic spheroid.[1]

A typical model is shown in Figure 8 for a prolate spheroid with an aspect ratio of a / b. The particle is assumed to be a metallic ellipsoid with a fluorophore positioned near the particle. The fluorophore is located outside the particle at a distance r from the center of the spheroid and a distance d from the surface. The fluorophore is located on the major axis and can be oriented parallel or perpendicular to the metallic surface.
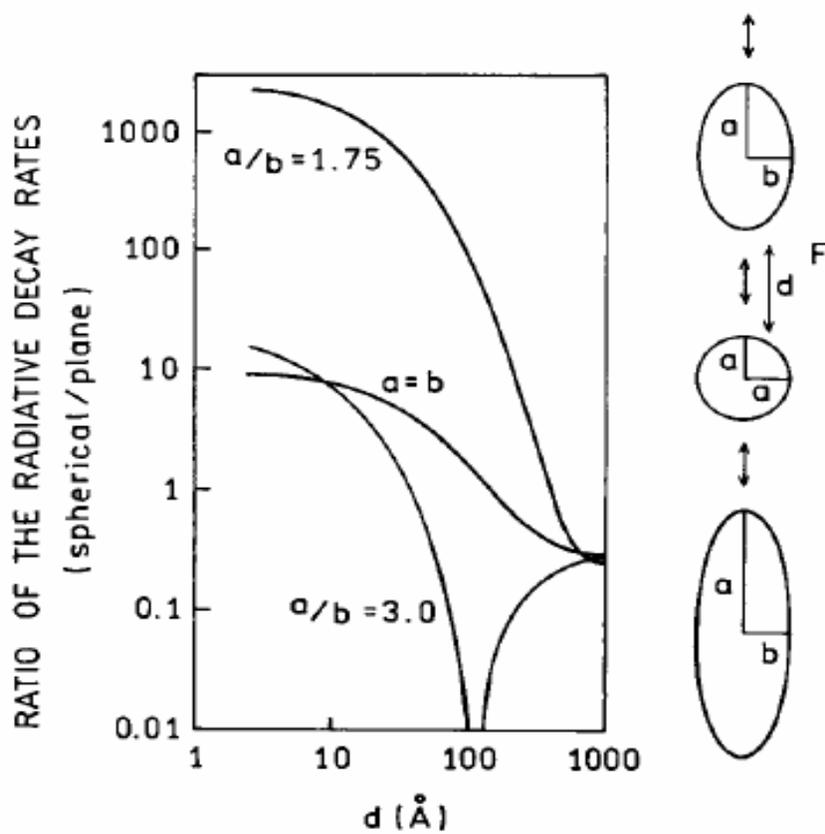
Figure 9. Effect of a metallic spheroid on the radiative decay rate of a fluorophore.
The resonant frequency of the dye is assumed to be 25,600 cm^{-1},approximately equal to
391nm. The volume of the spheroids is equal to that of a sphere with a radius of 200A$^{\circ}$.[1]

Figure 9 shows the radiative rates expected for a fluorophore at various

distance from the surface of a silver particle and for different orientations of the

fluorophore transition moment. The most remarkable effect is for a fluorophore

perpendicular to the surface of a spheroid with a / b = 1.75. In this case the radiative rate

can be enhanced by a factor of 1000-fold or greater. The effect is much smaller for a

sphere (a / b = 1.0), and much smaller for a more elongated spheroid (a / b = 3.0) when

the optical transition is not in resonance with the particle. In this case the radiative decay

rate can be decreased by over 100-fold. If the fluorophore displays a high quantum yield

or small value of k_{nr}, this effect could result in 100-fold longer lifetimes. The magnitude

of these effects depends on the location of the fluorophore around the particle and the orientation of its dipole moment relative to the metallic surface. The dominant effect of the perpendicular orientation is thought to be due to an enhancement of the local field along the long axis along the particle.
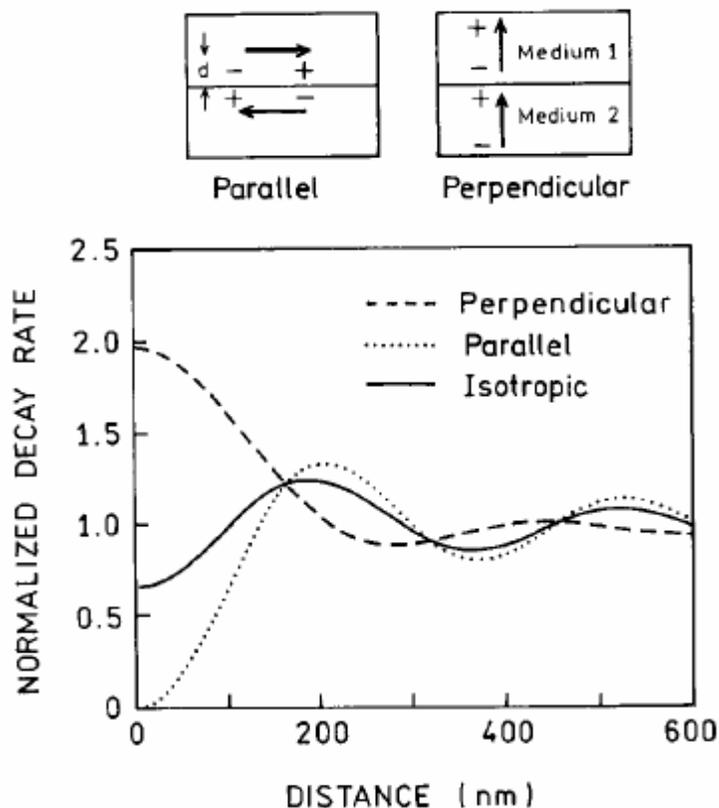
Figure 10. Effect of fluorophore orientation on the decay rate of a fluorophore near a metallic surface.[1]

The transition dipole-surface orientation can result in unusual effects. This is illustrated in Figure 10, which shows the expected decay rates of a fluorophore near solid silver surface[7]. The decay depends on orientation relative to the surface. In the parallel orientation the dipole in the metal cancels the dipole in the fluorophore, which slows the decay. In the perpendicular orientation the fluorophore's dipole and the dipole in the metal are synergistic and increase the decay rate.

15

1.4 Two Photon Photodynamic Cancer Therapy (PDT)

Perhaps the most successful integration of photonics and therapeutics is photodynamic therapy (PDT). PDT involves the administration of light-activated drugs (photosensitizer PS) that preferentially accumulate in tumors or rapidly developing blood vessels. Absorption of light by the PS generates a cytotoxic species such as reactive singlet oxygen which leads to irreversible destruction of the treated tissue. The light activation of these PS is based on linear optical excitation, using UV to NIR wavelengths, and this modality is known as one photon or single photon PDT. However, single photon PDT has important limitations. The use of alternative light activating methods using simultaneous two-photon excitation (TPE) has proved to be an excellent way to overcome the single photon PDT limitations and to increase selectivity. Two-photon PDT is based on the simultaneous absorption of two visible or near infra red (NIR) photons, which together provide the energy normally imparted upon absorption of a single photon of UV or visible light.

Some of the advantages of the two-photon PDT is that it allows the irradiation at wavelengths that do not coincide with the dominant one-photon transition. It reduces scattering and absorptivity in the NIR and improves depth of penetration in optically dense media such as tissue. It also reduces side effects attributable to absorption of radiation by the medium, and improves three dimensional control of photoactivation.

Hence, a driving motivation currently exists in advancing the research and development of two-photon based PDT through synthesis, characterization and screening of new, highly efficient, NIR two-photon absorbing dyes.

Our group has been involved with the design and synthesis of fluorene derivatives that posses high two-photon absorption (2PA) cross sections (δ).[26-28] Systematic variation of molecular structure has been accomplished, providing derivatives of varying electronic character (Figure 11).
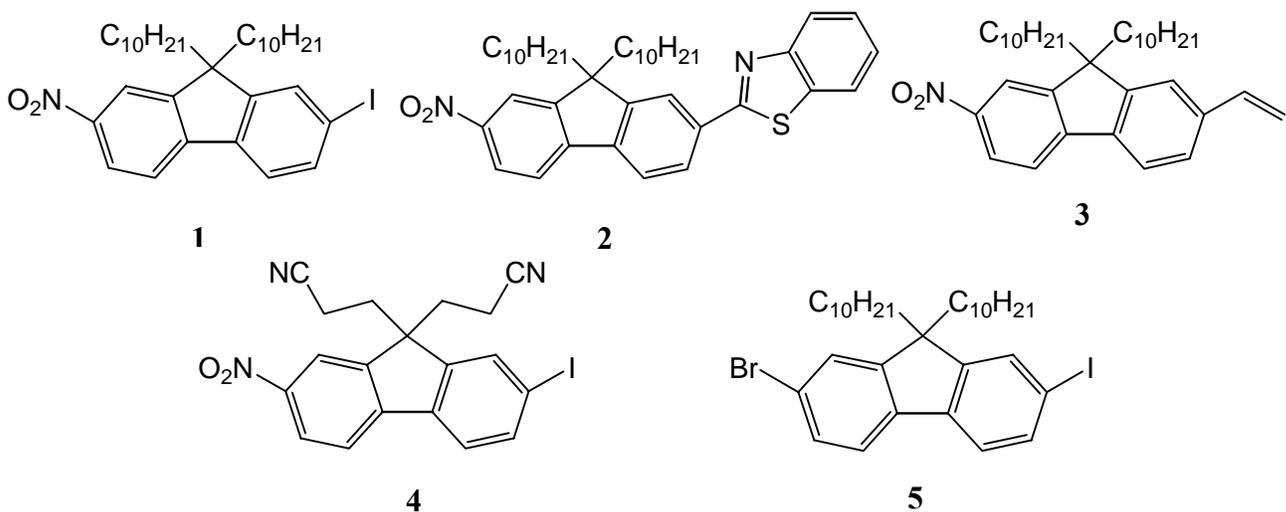
Figure 11. Structures of two photon absorbing fluorene derivatives.

Some of these derivatives incorporate heavy atoms and are particularly interesting for PDT due to the increase in the rate of intersystem crossing (ISC) to the triplet excited state, necessary for singlet oxygen sensitization. These derivatives posses high singlet oxygen quantum yields (Φ_Δ)[29] as shown in Table 1.

Table 1. Singlet oxygen quantum yields of fluorene derivatives.

Compound	λ (nm)	Solvent	Φ_Δ Measured (DPBF)
1	344	ethanol	O.42 ± 0.08
2	362	ethanol	0.61 ± 0.12
3	357	ethanol	0.59 ± 0.11
4	331	ethanol	0.65 ± 0.16
5	314	ethanol	0.86 ± 0.17

1.5 Fluorene Functionalized Gold Nanoparticles

Nanoparticles exhibit unique electronic, magnetic and optical properties because of their small size and large surface to volume ratio.[30,31] The synthesis of gold nanoparticles has been shown to take place via the reduction of HAuCl4 in the presence of alkanethiols.[32-35] Recently, there has been an increasing number of reports on the preparation and utilization of such thiol-stabilized gold nanoparticles, often referred to as monolayer-protected clusters (MPC).[36] Potential applications of these types of systems include optical devices, microelectronics, catalysts and chemical recognition.[37]

Fox et al have prepared fluorenyl-alkane-1-thiolate monolayer protected gold clusters (Au-MPCs) containing alkyl chains with different number of carbon atoms (Figure 12).[38,39] The strong fluorescence emission quenching of the fluorenyl-alkane-1-thiolate Au-MPCs compared to the optically matched solution of homogeneously dispersed fluorenyl thiol and alkane-1-thiolate Au-MPCs was attributed to the covalent

attachment of the fluorenyl probe to the gold clusters, thus facilitating strong through-

bond electronic coupling. They had proven that photoinduced energy transfer as the

principle mode for electronic coupling between the excited fluorenyl group and the

included gold clusters. Electronic coupling of the excited fluorenyl groups with the gold

core in these composite clusters affected the observed gold electron relaxation dynamics,

likely by adding an excitation path for gold electrons by working as a sensitizer.
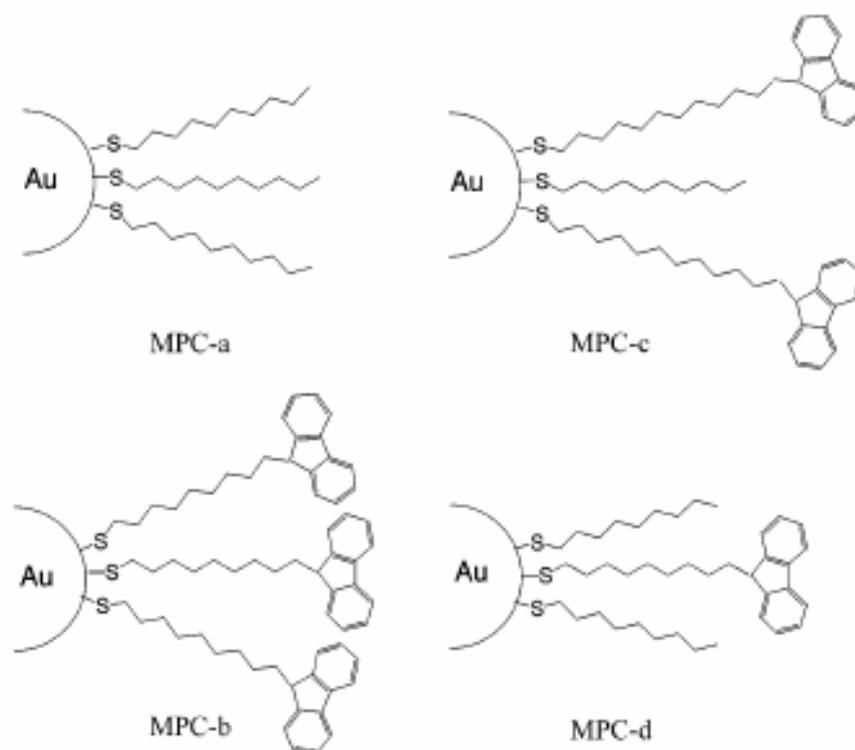
Figure 12. Partial structures of Monolayer-Protected Clusters (MPCs), capped by (a) Nonane-1-thiol, (b) 9-(9-Fluorenyl)-nonane-1-thiol, (c) Mixed monolayer of 9-(9-Fluorenyl)-dodecane-1-thiol and Nonane-1-thiol, and (d) Mixed monolayer of 9-(9-Fluorenyl)-nonane-1-thiol and Nonane-1-thiol.[38]

1.6 Applicability of RDE for two photon PDT

While a lot of groups have investigated the metal enhanced fluorescence of weakly fluorescent dyes, there have been no examples where the principles of RDE have been employed to explore the possibility of enhanced singlet oxygen sensitization by dyes that already exhibit a very high rate of intersystem crossing and high two photon absorption cross-sections.

Also to the best of our knowledge, there have been no examples in literature where metallic nanoparticles have been used as agents for electric-field enhancement (produced by the quantized oscillation of collective electrons in a plasma surface i.e. surface plasmon) to probe the rate of intersystem crossing in fluorene based photosensitizers which is the most important criteria for the dye to be used as a singlet oxygen sensitizer in PDT.

The primary aim of this research is to develop the synthetic methodology for functionalizing gold nanoparticles with two photon absorbing fluorene dyes (Table 1) possessing structural motifs that have been investigated by our group and proven to be excellent non-linear optical materials. In order to accomplish this, there was a need to incorporate thioalkyl chains which have different number of carbon atoms at the 9 position of the fluorene ring system containing different types of electron donating and electron accepting groups. These hybrid materials would be used to establish the foundation for radiative decay engineering (RDE) by combining surface plasmon enhancement effects with nonlinear optical processes such as multiphoton absorption, energy transfer and excited state intersystem crossing.

CHAPTER TWO: EXPERIMENTAL - SYNTHESIS AND CHARACTERIZATION OF FLUORENYL DERIVATIVES.

The reactions were conducted under nitrogen or argon atmospheres. All reagents were used as received from commercial suppliers. Potassium thioacetate was stored and handled in a glove box. ^{1}H and ^{13}C NMR spectra were recorded using a Varian Gemini 300 NMR spectrometer at 300 and 75 MHz respectively. Chemical shifts were interpreted using a computer modeling program in CS ChemDraw Ultra version 5.0 by CambridgeSoft corporation. Elemental analyses were carried out by Atlantic Microlabs.

2.1 Synthesis of 2-nitrofluorene (1).

Fluorene (60 g, 361 mmol) and 500 mL AcOH were heated, under N_2, to 50 °C in 1 L three-necked flask fitted with a thermometer and addition funnel. Nitric acid (80 mL) was added over 20 min via addition funnel. The temperature was raised to 85 °C and maintained for 5 min. The reaction mixture was removed from the heat and allowed to cool to room temperature over 2 h, resulting in a yellow suspension. This was filtered, washed with 50 mL AcOH containing 1.3 g KOAc, then slurried in water and filtered. The yellow product was dried in a vaccum oven, affording 58 g (77% yield). The melting point was 155-158 °C. (lit 160-163 °C).[40]

2.2 Synthesis of 7-iodo-2-nitrofluorene (2).

2-Nitrofluorene (6.4 g, 30 mmol) and 200 mL AcOH were stirred at room temperature in a 500 mL three-necked flask fitted with N_2 inlet, condenser, stir bar, and

stopper. I_2 (3.74 g, 14.7 mmol) was added to the reaction mixture and stirred for 20 min. An orange-brown liquid formed with some undissolved starting material remaining suspended. Sulfuric acid (20 mL) and 2.2 g sodium nitrite were then added, and the reaction mixture was heated to 115 °C for 1 h. Yellow precipitate formed, upon which the suspension was cooled to room temperature and poured into 200 g ice, filtered, washed with water, and dried in a vacuum oven. The crude product (9 g) was recrystallized from toluene, resulting in 7.5 g (74 % yield) of yellow needles. The melting point was 245-246 °C. (lit 244-245 °C).[41]

2.3 Synthesis of 9, 9-bis-(6-bromo-hexyl)-2-iodo-7-nitro-9*H*-fluorene (3).

To a 100 mL three-necked round bottom flask containing 7-iodo-2-nitrofluorene (2 g, 5.93 mmol), 1, 6-dibromohexane (9.10 mL, 59.3 mmol), 27.66 mL toluene, and 0.088 g tetrabutylammonium bromide (TBAB), as a phase-transfer catalyst, was added 27.66 mL of 50 wt % sodium hydroxide solution. This two phase mixture was refluxed at 100 °C with vigorous stirring and bubbling nitrogen gas. The reaction progress was monitored by TLC (5% EtOAc/hexanes). When the starting compound, 7-iodo-2-nitrofluorene, had completely disappeared (after 4 h), the reaction mixture was poured into toluene and then washed with water (x 2) to remove the excess sodium hydroxide. The organic layer was separated, dried over $MgSO_4$, and concentrated by solvent evaporation. Purification was accomplished by column chromatography using silica gel. Initially, hexane was used as the solvent in order to remove the excess 1, 6-dibromohexane, followed by elution with 5% EtOAc/hexanes, providing 2 g of viscous yellow oil that crystallized upon standing (51% yield). The melting point was 93 – 95 °C.

. Elemental analysis for $C_{25}H_{30}Br_2INO_2$: Anal. calcd: 45.27% C, 4.56% H, 24.10% Br, 2.11% N; Found: 45.34% C, 4.58% H, 23.82% Br, 2.18% N; ^{1}H NMR (300 MHz, CDCl$_3$) δ: 8.25 (d, 1H, ArH), 8.16 (s, 1H, ArH), 7.79 (s, 1H, ArH), 7.72 (d, 2H, ArH), 7.52 (d, 1H, ArH), 3.29 (t, 4H, CH$_2$Br), 2.0 (m, 4H, CH$_2$), 1.65 (m, 4H, CH$_2$), 1.18 (m, 8H, CH$_2$), 0.6 (m, 4H, CH$_2$); ^{13}C NMR (75 MHz, CDCl$_3$) δ: 154.19, 151.17, 147.73, 146.69, 138.48, 136.95, 132.59, 123.77, 123.02, 120.36, 118.38, 95.94, 56.11, 40.19, 34.22, 32.92, 29.27, 28.13, 23.93;

2.4 Synthesis of 9, 9-bis-(10-bromodecyl)-2-iodo-7-nitro-9*H*-fluorene (4).

To a 100 mL three-necked round bottom flask containing 7-iodo-2-nitrofluorene (3 g, 8.9 mmol), 1, 10-dibromohexane (20 mL, 89 mmol), 41.5 mL toluene, and 0.132 g tetrabutylammonium bromide (TBAB), as a phase-transfer catalyst, was added 41.5 mL of 50 wt % sodium hydroxide solution. This two phase mixture was refluxed at 100 °C with vigorous stirring and bubbling nitrogen gas. The reaction in progress was monitored by TLC (2.5% EtOAc/hexanes). When the starting compound 7-iodo-2-nitrofluorene had completely disappeared after 4 h, the reaction mixture was poured into toluene and then washed with water (x 2) to remove the excess sodium hydroxide. The organic layer was separated, dried over MgSO$_4$, and concentrated by solvent evaporation. Purification was accomplished by column chromatography using silica gel. Initially, hexane was used as the solvent in order to remove the excess 1, 10-dibromohexane followed by elution with 2.5% EtOAc/hexanes, providing 2.9 g of viscous yellow oil that crystallized upon standing (43% yield). The melting point was 48 – 50 °C. Elemental analysis for $C_{33}H_{46}Br_2INO_2$: Anal. calcd: 51.11% C, 5.98% H,

23

20.61% Br, 1.81% N; Found: 50.92% C, 6.05% H, 20.36% Br, 1.85% N; ^{1}H NMR (

300MHz, CDCl$_3$) δ: 8.25 (d, 1H, ArH), 8.16 (s, 1H, ArH), 7.78 (s, 1H, ArH), 7.72 (d, 2H,

ArH), 7.53 (d, 1H, ArH), 3.38 (t, 4H, CH$_2$Br), 2.0 (m, 4H, CH$_2$), 1.81 (m, 4H, CH$_2$), 1.36

(m, 4H, CH$_2$), 1.09 (m, 24H, CH$_2$), 0.58 (m, 4H, CH$_2$); ^{13}C NMR (75 MHz, CDCl$_3$) δ:

154.54, 151.49, 147.66, 146.71, 138.49, 136.78, 132.66, 123.63, 122.94, 120.26, 118.44,

95.82, 56.23, 40.25, 34.48, 33.15, 30.07, 29.68, 29.64, 29.46, 29.03, 28.48, 24.03.

2.5 Synthesis of [(6-{2-iodo-9-[6-(methyl-oxomethylene-λ[4]-sulfanyl)-hexyl]-7-nitro-9*H*-luoren-9-yl}-hexyl)-methyl- λ[4]-sulfanylidene]-methanone (5).

To a 50 mL three necked round bottom flask was added **3** (0.8 g, 1.21 mmol),

potassium thioacetate (0.303 g, 2.7 mmol), and 24 mL 100% ethanol. The contents were

degassed under vacuum and nitrogen. The reaction mixture was refluxed under nitrogen.

The reaction in progress was monitored by TLC (5% EtOAc/hexanes). The starting

compound **3** completely disappeared after 2 h. Ethanol was removed by rotary

evaporation and the reaction mixture was extracted with dichloromethane, washed with

water (x 2), and then dried over MgSO$_4$. Purification was accomplished by column

chromatography using silica gel (5% EtOAc/hexanes), providing 0.64 g of viscous

yellow oil (yield 82 %). Elemental analysis for C$_{29}$H$_{36}$INO$_4$S$_2$: Anal. calcd: 53.29% C,

5.55% H, 9.81% S, 2.14% N; Found: 53.15% C, 5.52% H, 9.72% S, 2.29% N; ^{1}H NMR (

300 MHz, CDCl$_3$) δ: 8.19 (d, 1H, ArH), 8.08 (s, 1H, ArH), 7.70 (s, 1H, ArH), 7.63 (d,

2H, ArH), 7.45 (d, 1H, ArH), 2.66 (t, 4H, CH$_2$S), 2.20 (s, 6H, CH$_3$), 1.93 (m, 4H, CH$_2$),

1.30 (m, 4H, CH$_2$), 1.02 (m, 8H, CH$_2$), 0.47 (m, 4H, CH$_2$); ^{13}C NMR (75 MHz, CDCl$_3$) δ:

196.04, 154.29, 151.25, 147.72, 146.67, 138.48, 136.88, 132.59, 123.71, 123.0, 120.32,

118.40, 109.89, 109.86, 109.83, 95.90, 56.13, 40.22, 31.02, 29.69, 29.61, 29.31, 28.72, 23.94.

2.6 Synthesis of [(10-{2-iodo-9-[10-(methyl-oxomethylene-λ^4-sulfanyl)-decyl]-7-nitro-9*H*-fluoren-9-yl}-decyl)-methyl- λ^4-sulfanylidene]-methanone (6).

To a 50 mL three-necked round bottom flask was added **4** (1.58 g, 2.03 mmol), potassium thioacetate (0.512 g, 4.5 mmol), and 40.6 mL 100% ethanol. The contents were degassed under vacuum and nitrogen. The reaction mixture was refluxed under nitrogen. The reaction progress was monitored by TLC (5% EtOAc/hexanes). The starting compound **4** completely disappeared after 2 h. Ethanol was removed by rotary evaporation and the reaction mixture was extracted with dichloromethane, washed with water (x 2), and then dried over $MgSO_4$. Purification was accomplished by column chromatography using silica gel (5% EtOAc/hexanes), providing 1.13 g of viscous yellow oil (yield 73 %). Elemental analysis for $C_{37}H_{52}INO_4S_2$: Anal. calcd: 58.03% C, 6.84% H, 8.37% S, 1.83% N; Found: 58.02% C, 6.64% H, 8.35% S, 2.02% N; ^{1}H NMR (300 MHz, $CDCl_3$) δ: 8.17 (d, 1H, ArH), 8.08 (s, 1H, ArH), 7.69 (s, 1H, ArH), 7.65 (d, 2H, ArH), 7.44 (d, 1H, ArH), 2.74 (t, 4H, CH_2S), 2.23 (s. 6H, CH_3), 1.91 (m, 4H, CH_2), 1.43 (m, 4H, CH_2), 1.07 (m, 24H, CH_2), 0.48 (m, 4H, CH_2); ^{13}C NMR (75 MHz, $CDCl_3$) δ: 196.07, 154.55, 151.51, 147.69, 146.68, 138.49, 136.77, 132.68, 123.61, 122.92, 120.23, 118.44, 95.80, 56.23, 40.23, 31.96, 31.01, 30.09, 29.82, 29.71, 29.67, 29.49, 29.37, 29.12, 24.05, 23.04, 14.54.

2.7 Synthesis of 6-[2-iodo-9-(6-mercapto-hexyl)-7-nitro-9*H*-fluoren-9-yl]-hexane-1-thiol (7).

To a 50 mL three-necked round bottom flask was added **5** (0.33 g, 0.5 mmol), 3 M sodium hydroxide solution (10.1 mL), and 5 mL 100% ethanol. The contents of the flask were refluxed for 2 days in order to ensure the complete hydrolysis of thioester to thiol. TLC (50% EtOAc/hexanes) was used to monitor the progress of the reaction. Ethanol was removed using rotary evaporation. The reaction mixture was extracted with dichloromethane, washed with 1 M hydrochloric acid, water, and then dried over $MgSO_4$. The crude product (0.1 g, 35% yield) was used without further purification. ^{1}H NMR (300 MHz, $CDCl_3$) δ: 8.18 (d, 1H, ArH), 8.07 (s, 1H, ArH), 7.66 (m, 3H, ArH), 7.41 (d, 1H, ArH), 2.41 (t, 4H, CH_2S), 1.90 (m, 4H, CH_2), 1.36 (m, 4H, CH_2), 1.02 (m, 8H, CH_2), 0.46 (m, 4H, CH_2); ^{13}C NMR (75 MHz, $CDCl_3$) δ: 154.31, 151.28, 147.72, 146.67, 138.48, 136.88, 132.61, 123.71, 122.99, 120.32, 118.40, 95.91, 56.14, 40.20, 39.13, 31.32, 31.01, 30.08, 29.70, 29.60, 29.27, 28.71, 28.38, 23.97.

2.8 Synthesis of 10-[2-iodo-9-(10-mercapto-decyl)-7-nitro-9*H*-fluoren-9-yl]-decane-1-thiol (8).

To a 50 mL three-necked round bottom flask was added **6** (0.66 g, 0.862 mmol), 3 M sodium hydroxide solution (17.2 mL), and 8.6 mL 100% ethanol. The contents of the flask were refluxed for 2 days in order to ensure the complete hydrolysis of thioester to thiol. TLC (50% EtOAc/hexanes) was used to monitor the progress of the reaction. Ethanol was removed using rotary evaporation. The reaction mixture was extracted with dichloromethane, washed with 1 M hydrochloric acid, water, and then

26

dried over MgSO$_4$. The crude product (0.15 g, 26% yield) was used without further purification. ^{1}H NMR (300 MHz, CDCl$_3$) δ: 8.17 (1H, d, ArH), 8.08 (1H, s, ArH), 7.65 (3H, m, ArH), 7.44 (1H, d, ArH), 2.55 (4H, t, CH$_2$S), 1.91 (4H, m, CH$_2$), 1.53 (4H, m, CH$_2$), 1.08 (24H, m, CH$_2$), 0.48 (4H, m, CH$_2$); ^{13}C NMR (75 MHz, CDCl$_3$) δ: 153.09, 150.04, 146.20, 145.25, 137.03, 135.31, 131.20, 122.17, 121.48, 118.80, 116.98, 94.39, 54.78, 38.80, 37.99, 28.65, 28.37, 28.27, 28.08, 27.92, 27.68, 27.39, 22.60.

2.9 Synthesis of 2-[9, 9-bis-(6-bromo-hexyl)-7-nitro-9*H*-fluoren-2-yl]-benzothiazole (9).

To a 25 mL three-necked round bottom flask containing 2-(7-nitro-9*H*-fluoren-2-yl)-benzothiazole (0.1 g, 0.29 mmol), 1, 6-dibromohexane (0.45 mL, 2.9 mmol), 1.35 mL toluene, and 0.004 g tetrabutylammonium bromide (TBAB), as a phase-transfer catalyst, was added 1.35 mL of 50 wt % sodium hydroxide solution. This two phase mixture was refluxed at 100 °C with vigorous stirring and bubbling nitrogen gas. The reaction in progress was monitored by TLC (2% EtOAc/hexanes). When the starting compound 2-(7-nitro-9*H*-fluoren-2-yl)-benzothiazole had completely disappeared after 4 h, the reaction mixture was poured into toluene and then washed with water (x 2) to remove the excess sodium hydroxide. The organic layer was separated, dried over MgSO$_4$, and concentrated by solvent evaporation. Purification was accomplished by column chromatography using silica gel. Initially, hexane was used as the solvent in order to remove the excess 1, 6-dibromohexane followed by elution with 2% EtOAc/hexanes, providing 0.09 g of viscous yellow oil that crystallized upon standing (45% yield)**.** The melting point was 141-144 °C. ^{1}H NMR (300 MHz, CDCl$_3$) δ: 8.30 (d,

1H, ArH), 8.21 (d, 2H, ArH), 8.08 (d, 2H, ArH), 7.86 (m, 3H, ArH), 7.49 (t, 1H, ArH), 7.41 (t, 1H, ArH), 3.24 (t, 4H, CH_2Br), 2.13 (m, 4H, CH_2), 1.63 (m, 4H, CH_2), 1.17 (m, 8H, CH_2), 0.61 (m, 4H, CH_2); ^{13}C NMR (75 MHz, $CDCl_3$) δ: 167.83, 152.95, 152.42, 147.85, 146.61, 141.52, 135.25, 134.63, 127.83, 126.77, 125.71, 123.76, 123.46, 122.0, 121.88, 120.76, 118.45, 56.30, 40.27, 34.13, 32.90, 29.28, 28.14, 24.01.

2.10 Attempted gold nanoparticle functionalization with compound (7)

An aqueous gold nanoparticle solution (3 mL, 5 nm) was stirred with 100 μL of compound **7** in toluene (0.13 M) and 60.5 μL of compound **7** in toluene (0.01 M) in two different 5 mL round bottom flasks for 4 days. The reaction progress was followed by UV-vis spectroscopy. After stirring, the reaction mixture was transferred to a 30 mL separatory funnel and extracted with 1 mL toluene. The two different organic layers were analysed using UV-vis and Raman spectroscopy.

CHAPTER THREE: RESULTS AND DISCUSSION OF FLUORENYL DERIVATIVES

A new synthetic methodology has been developed for imparting thioalkyl chains at the 9-position of the fluorene ring system containing different types of electron donating and accepting groups at the 2 and 7 positions. The thioalkyl chains were chosen due to the excellent affinity of the thiol group to gold. This was intended to enable the attachment of 7-iodo-2-nitrofluorene to gold nanoparticles and also retain the electronic character of the fluorene ring system. The aim was to investigate the impact of possible surface plasmon enhancement, generated by the gold nanoparticles, on the rate of intersystem crossing of the fluorene derivative which was already demonstrated to exhibit high singlet oxygen quantum yields and two photon absorption (2PA) cross-sections. The distance between the gold nanoparticles and the dye was adjusted by introducing thioalkyl chains that contain different number of carbon atoms (methylene spacers). For preliminary investigations, the intent was to introduce thioalkyl chains containing methylene spacers with six and ten carbons which will help in maintaining the distance between 7-iodo-2-nitrofluorene and gold nanoparticles at 9 Å and 14 Å respectively (CS Chem3D pro). This was desired in order to keep the fluorophore within the distance limit of 50 Å from the metal which is absolutely necessary for the metal to exhibit its fluorescence quenching property as shown in Figure 7 and investigate whether the possible surface plasmon enhancement generated by gold nanopartcicles increases the rate of intersystem crossing and thereby the singlet oxygen quantum yield. To the best of our knowledge, this is the first study undertaken on this aspect of photoreactivity in

correlation with the RDE studies carried out by Lackowicz *et al.* [1] on metal enhanced fluorescence.

The compounds synthesized were fully characterized using ^{1}H NMR, ^{13}C NMR and elemental analysis. The synthesis and characterization of the functionalized fluorene derivatives is followed by the presentation of preliminary results on the UV-vis spectra of gold nanoparticles functionalized using 6-[2-iodo-9-(6-mercapto-hexyl)-7-nitro-9H-fluoren-9-yl]-hexane-1-thiol (**7**).

.

2-Nitrofluorene (**1**) was prepared in 76% yield by regioselective nitration of fluorene with nitric acid in AcOH at 85 °C (Scheme 1). The melting point of 155-158 °C was in good agreement with the literature value (157 °C).

Scheme 1
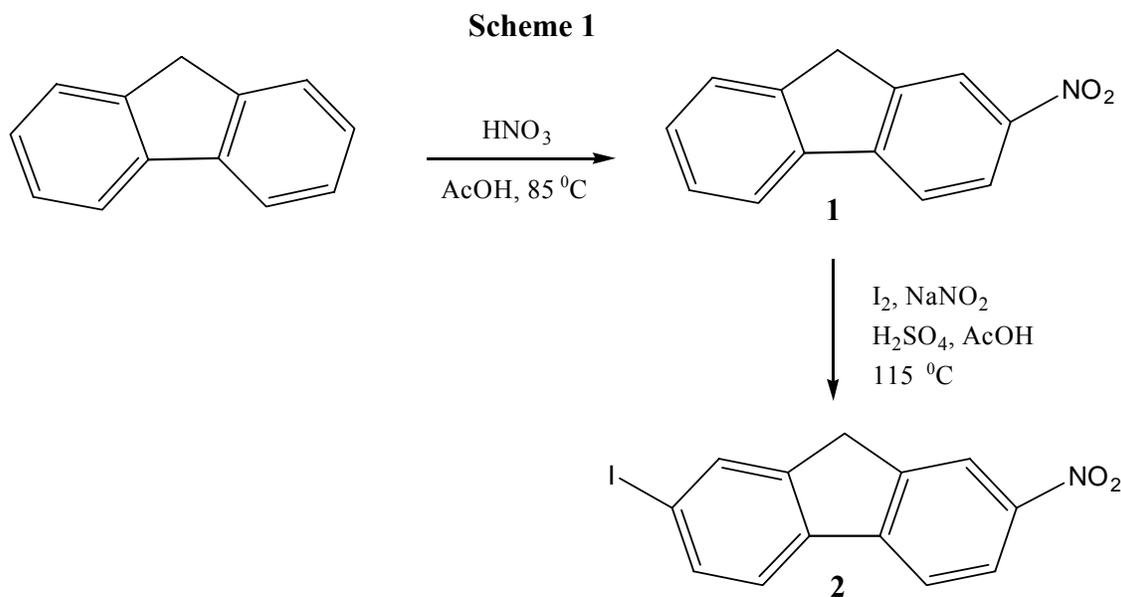
Regiospecific iodination of 2-nitrofluorene (**1**) with iodine, sodium nitrite, AcOH and H_2SO_4 at 115 °C, afforded 7-iodo-2-nitrofluorene (**2**) in 72% yield after recrystallization from toluene. Again, the melting point (245-248 °C) was consistent with the literature value (244-245 °C).

3.1 Dialkylation using α, ω-dibromoalkane

The dialkylation of 7-iodo-2-nitrofluorene (**2**) using α, ω-dibromoalkane, Br(CH$_2$)$_n$Br (n = 6, 10) was accomplished using a biphasic reaction mixture involving toluene and aqueous sodium hydroxide solution (50 wt%), as shown in Scheme 2. Tetrabutylammo- nium bromide (TBAB) was used as the phase transfer catalyst.[42] A ten-fold excess molar equivalent of the dibromoalkane was used over 7-iodo-2-nitrofluorene in order to restrain the attack of the fluorenyl anion exclusively on one of the carbon atoms of the dibromoalkane bearing a bromine. The reaction mixture was refluxed at 100 °C and the progress of the reaction was monitored using TLC. The reaction was complete in 4 h once all of **2** had disappeared.

Scheme 2
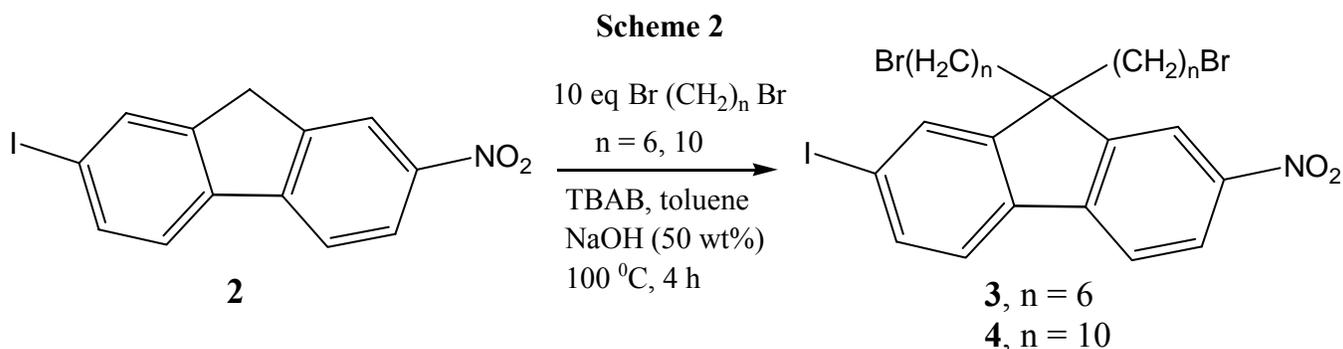
3.1.1 9, 9-Bis-(6-bromo-hexyl)-2-iodo-7-nitro-9*H*-fluorene (3).

The general procedure described above was followed and work up was done by first performing an extraction with toluene and water. Toluene was by removed by distillation under reduced pressure. The crude product was then purified by column chromatography. Initially, hexane was used as the solvent in order to remove the excess 1, 6-dibromohexane followed by 5% EtOAc/hexanes providing a viscous yellow oil that yielded yellow crystals upon standing (mp 93- 95 °C). The product was characterized

using ^{1}H NMR, ^{13}C NMR, and elemental analysis. The ^{1}H NMR data (Figure 14) indicated a pure product with a characteristic peak at 3.29 ppm (t, 4H), representing the protons adjacent to bromine atom on the alkyl chains. The peak corresponding to the carbon adjacent to the bromine atom was present at 40.19 ppm (Figure 15).
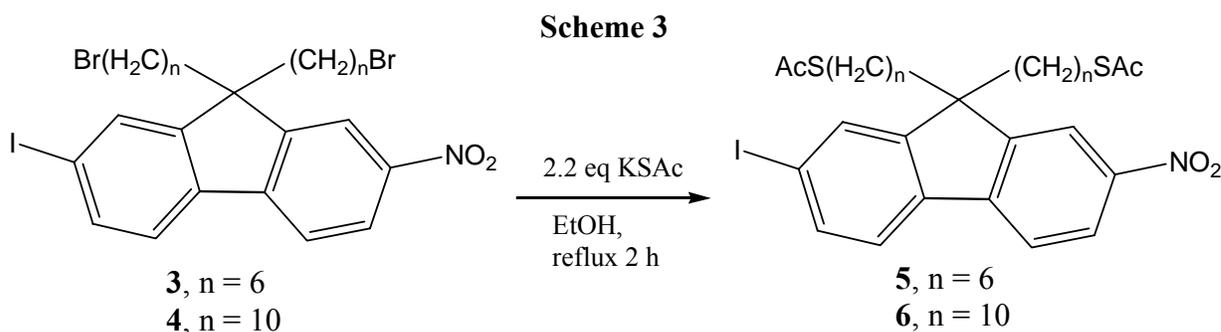
3.1.2. 9, 9-Bis-(10-bromo-decyl)-2-iodo-7-nitro-9*H*-fluorene (4).

The general procedure described above was followed and work up was done by first performing an extraction with toluene and water. Toluene was by removed by distillation under reduced pressure. The crude product was then purified by column chromatography. Initially, hexane was used as the solvent in order to remove the excess 1, 10-dibromohexane followed by elution with 2.5% EtOAc/hexanes, providing a viscous yellow oil that yielded pale yellow crystals upon standing (mp 47-49 °C). The product was characterized using ^{1}H NMR, ^{13}C NMR and elemental analysis. The ^{1}H NMR data (Figure 16) indicated a pure product with a characteristic peak at 3.38 ppm (t, 4H) which represents the protons adjacent to bromine atom on the alkyl chains. The peak corresponding to the carbon adjacent to bromine atom was present at 40.25 ppm (Figure 17).

3.2. Reaction with potassium thioacetate

The bromines on the alkyl chains of **3** and **4** were converted to thioester by reaction with potassium thioacetate as illustrated in Scheme 3. The thioester functionality provides one of the most facile means for conversion to thiols.[43] Potassium thioacetate is one of the most commonly used reagents reported in literature for conversion of halides

to thioesters. The reaction involved addition of 2.2 molar equivalents of potassium

thioacetate to a 0.05 M solution of 9, 9-bis-(6-bromo-alkyl)-2-iodo-7-nitro-9*H*-fluorene

(**3**, **4**) in 100% ethanol. The reaction mixture was refluxed at 75 °C and the progress of

the reaction was monitored by TLC. The reaction was complete in 2 h once all of 9, 9-

bis-(6-bromo-alkyl)-2-iodo-7-nitro-9*H*-fluorene (**3**, **4**) was consumed.

Scheme 3

2.2 eq KSAc

EtOH,
reflux 2 h

3, n = 6
4, n = 10

5, n = 6
6, n = 10

3.2.1 [(6-{2-Iodo-9-[6-(methyl-oxomethylene-λ^4-sulfanyl)-hexyl]-7-nitro-9*H*-fluoren-9-yl}-hexyl)-methyl- λ^4-sulfanylidene]-methanone (5)

The general procedure described above was followed and work up was done by

first distilling ethanol under reduced pressure, followed by extraction with

dichloromethane and washing with water. The crude product was then purified by

column chromatography using 2.5% EtOAc/hexanes as solvent, providing a viscous

yellow oil. The product was characterized using ^{1}H NMR, ^{13}C NMR, and elemental

analysis. The ^{1}H NMR data (Figure 18) indicated a pure product with the peak

corresponding to protons adjacent to bromine atoms of the dialkyl chains of **3** shifting

upfield to 2.66 ppm (t, 4H) and the formation of a new methyl resonance at 2.20 ppm (s,

6H). Conclusive proof was obtained from ^{13}C NMR (Figure 19) with the observation of a carbonyl carbon peak (C = O) at 196.04 ppm.
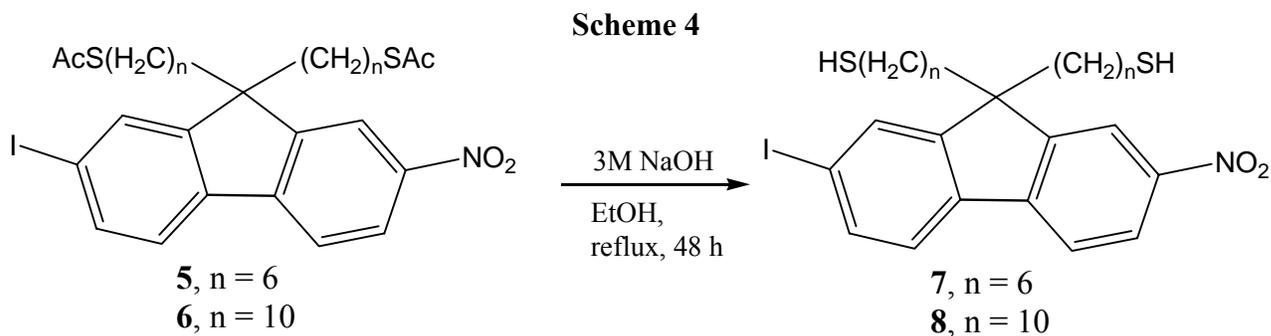
3.2.2 [(6-{2-Iodo-9-[6-(methyl-oxomethylene-λ^4-sulfanyl)-decyl]-7-nitro-9*H*-fluoren-9-yl}-decyl)-methyl- λ^4-sulfanylidene]-methanone (6)

The general procedure described above was followed and work up was done by first distilling ethanol under reduced pressure followed by extraction with dichloromethane and washing with water. The crude product was then purified by column chromatography using 1.5% EtOAc/hexanes as solvent, providing a viscous yellow oil. The obtained product was characterized using ^{1}H NMR, ^{13}C NMR, and elemental analysis. The ^{1}H NMR data (Figure 20) indicated a pure product with the peak corresponding to protons adjacent to bromine atoms of the dialkyl chains of **4** shifting upfield to 2.74 ppm (t, 4H) and the formation of a new methyl peak at 2.23 ppm (s, 6H). Conclusive proof was obtained from ^{13}C NMR (Figure 21) with the formation of a carbonyl carbon peak (C = O) at 196.07 ppm.

3.3. Hydrolysis of thioester to thiol

The thioester functionality on the alkyl chains was converted to thiol by means of a base hydrolysis using 3 M sodium hydroxide solution,[43] as shown in Scheme 4. The reaction involved addition of aqueous 3 M sodium hydroxide to 0.1 M solution of [(6-{2-iodo-9-[6-(methyl-oxomethylene-λ^4-sulfanyl)-alkyl]-7-nitro-9*H*-fluoren-9-yl}-alkyl)-methyl- λ^4-sulfanylidene]-methanone (**5**, **6**) in 100% ethanol. The contents of the flask

were refluxed at 75 °C and the progress of the reaction was monitored by TLC. The

reaction was complete in 2 days when most of the starting material had disappeared. The

yield was lower than expected due to precipitation of disulfides during the course of

reaction.

Scheme 4

AcS(H₂C)ₙ ... (CH₂)ₙSAc

I— ...—NO₂

5, n = 6
6, n = 10

3M NaOH
EtOH,
reflux, 48 h

HS(H₂C)ₙ ... (CH₂)ₙSH

I— ...—NO₂

7, n = 6
8, n = 10

### 3.3.1 6-[2-Iodo-9-(6-mercapto-hexyl)-7-nitro-9*H*-fluoren-9-yl]-hexane-1-thiol (7)

The general procedure described above was followed and work up was done by

first distilling ethanol under reduced pressure, followed by extraction with

dichloromethane and washing with 1M hydrochloric acid followed by water. The

disulfides that precipitated were filtered off by vacuum filtration. The crude product was

used without further purification and characterized using ¹H and ¹³C NMR. The ¹H NMR

data (Figure 22) indicated an almost pure product with the methyl peak corresponding to

the thioester nearly gone and protons adjacent to the thioester functionality of the dialkyl

chains shifting upfield to 2.41 ppm from 2.66 ppm. The ¹³C NMR (Figure 23) indicated

that the peak corresponding to the carbonyl carbon (C = O) at 196.04 ppm had almost

disappeared, a clear indication of hydrolysis.

3.3.2 10-[2-Iodo-9-(10-mercapto-decyl)-7-nitro-9*H*-fluoren-9-yl]-decane-1-thiol (8).

The general procedure described above was followed and work up was done by first distilling ethanol under reduced pressure, followed by extraction with dichloromethane and washing with 1M hydrochloric acid followed by water. The disulfides that precipitated were filtered off by vacuum filtration. The crude product obtained was used without further purification and characterized using ^{1}H and ^{13}C NMR. The ^{1}H NMR data (Figure 24) indicated an almost pure product with the methyl peak corresponding to the thioester nearly gone and protons adjacent to the thioester functionality of the dialkyl chains shifting upfield to 2.55 ppm from 2.74 ppm. The ^{13}C NMR (Figure 25) indicated that the peak corresponding to the carbonyl carbon ($C = O$) at 196.07 ppm had almost disappeared, again an indication of near complete hydrolysis.

3.4. Applicability to other fluorene derivatives

In order to verify the applicability of this synthetic methodology to the synthesis of other fluorene derivatives with substituents other than iodo- and nitro- groups at the 2 and 7 positions, the dialkylation procedure using dibromohexane was carried out on 2-(7-nitro-9*H*-fluoren-2-yl)-benzothiazole.

Scheme 5
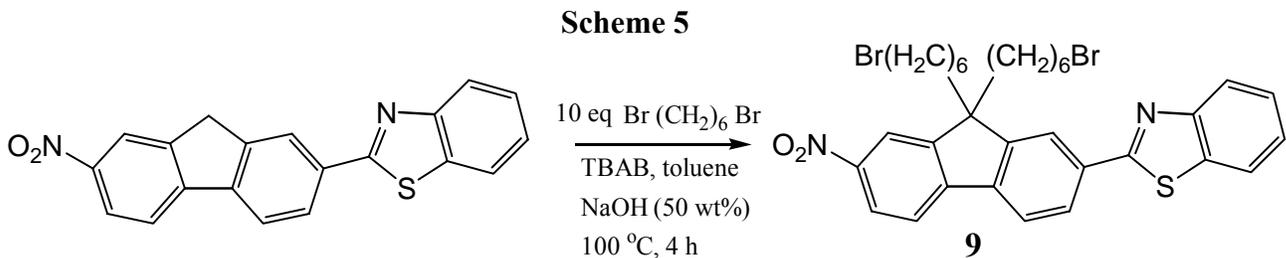
The general procedure described in Section 3.1 was followed and work up was done by first performing an extraction with toluene and water. Toluene was by

removed by distillation under reduced pressure. The crude product was then purified by column chromatography. Initially, hexane was used as the solvent in order to remove the excess 1, 6-dibromohexane followed by elution with 2% EtOAc/hexanes providing a viscous yellow oil that yielded yellow crystals upon standing (mp 141 – 144 °C). The product was characterized using ^{1}H and ^{13}C NMR. The ^{1}H NMR data (Figure 26) indicated a pure product with a characteristic peak at 3.24 ppm (t, 4H), representing the protons adjacent to bromine atom of the alkyl chains. The ^{13}C NMR (Figure 27) indicated the presence of the peak corresponding to carbon adjacent to bromine atom at 40.27 ppm as well as the resonance of the carbon in the 2-position in the bezothiazole ring at 167.83 ppm.

Currently efforts focus on the conversion of the bromoalkyl chain on compound **9** to thioalkyl moiety and investigate the enhancement in its singlet oxygen quantum yields due to possible surface plasmon enhancement generated by its attachment to gold nanoparticles. Efforts also focus on the reduction of the nitro group in compound **9** to the amine group, and eventually carrying out the introduction of diphenyl amino (-NPh$_2$) functionality through an Ullmann-type condensation reaction. This will enable the attachment of thioalkyl chains to the fluorene ring system with diphenylamino- and benzothiazole- functionalities at 2 and 7 positions, respectively.

3.5. Functionalization of gold nanoparticles.

Functionalization of gold nanoparticles was attempted using two different concentrations of compound **7** (0.13 M and 0.01 M in toluene). Unfortunately, even after 4 days of stirring with aqueous gold nanoparticle solutions (5 nm), the anticipated color

change (reddish pink), due to transfer of gold nanoparticles from the aqueous phase to toluene, was not observed. The two organic layers were analysed using UV-vis and Raman spectroscopy. The UV-vis spectrum did not reveal the presence of the anticipated surface plamon peak of gold nanoparticle at 520-535 nm (Figure 13). The Raman spectrum also did not show any conceivable enhancement in the signal due to presence of the metallic particles.
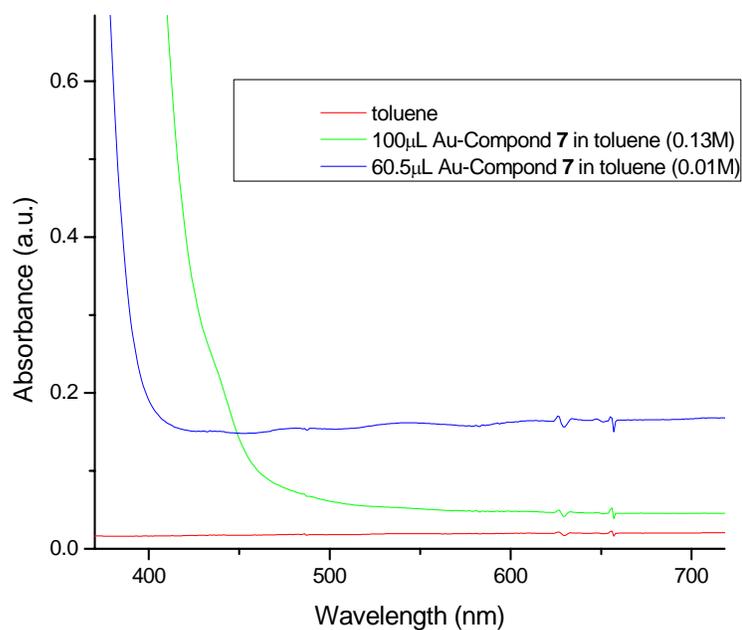

Figure 13. UV-vis spectrum of Au-compound 7 (0.13 M) and Au-compound 7 (0.01M) in toluene.
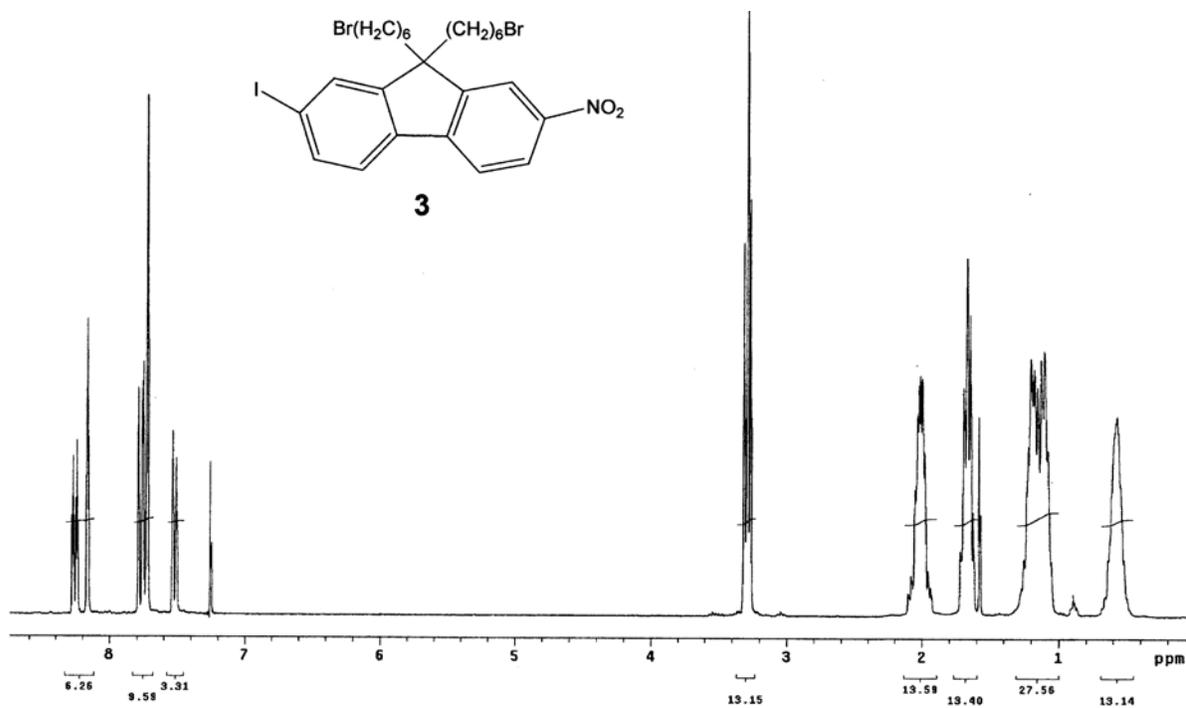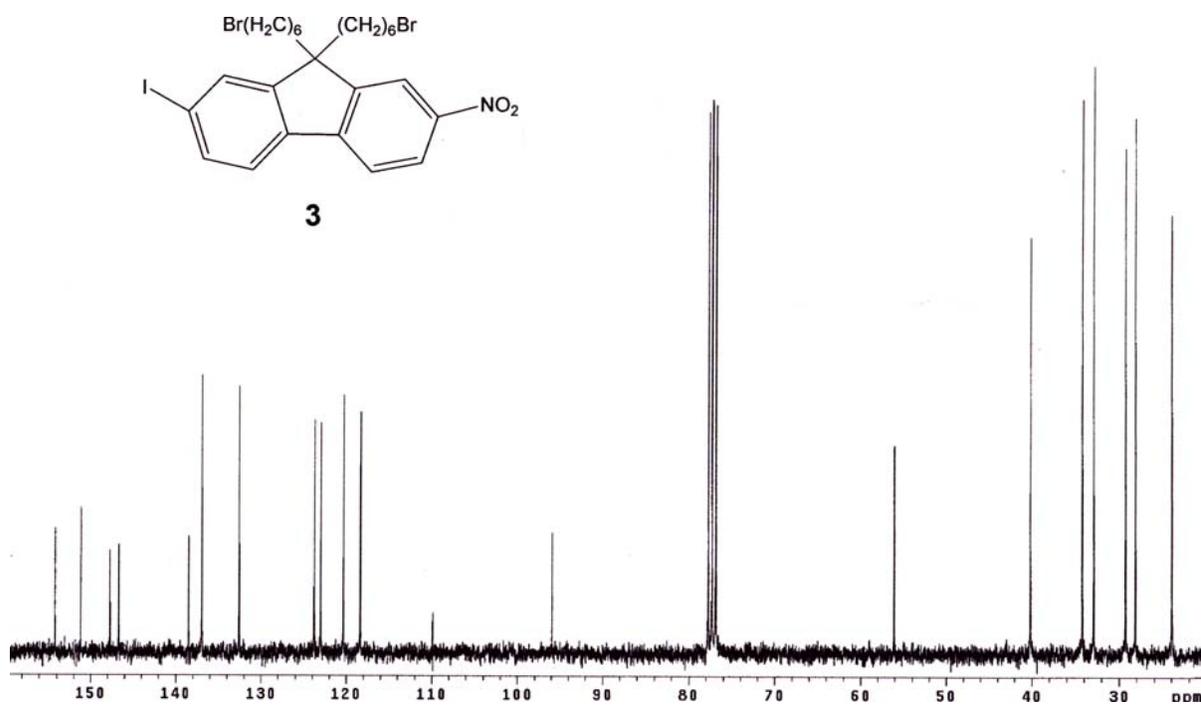
Figure 14. ^{1}H NMR spectrum of compound **3**.
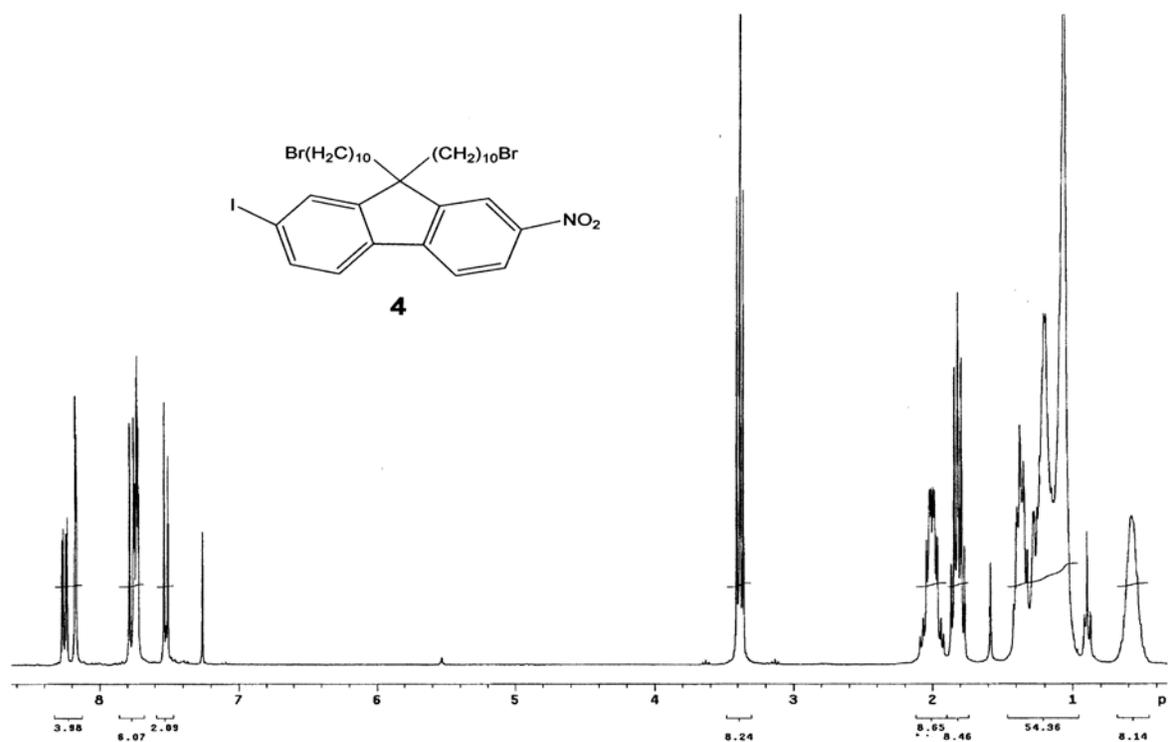

Figure 15. ^{13}C NMR spectrum of compound **3**.

Figure 16. ^{1}H NMR spectrum of compound **4**.
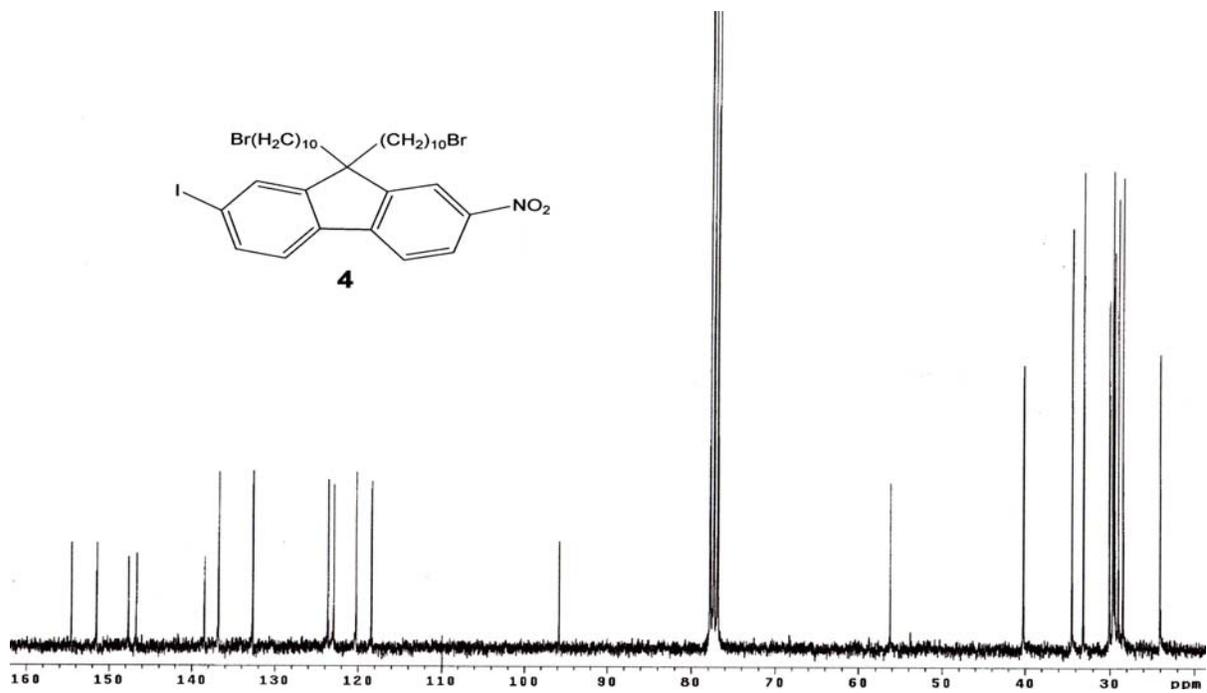
Figure 17. ^{13}C NMR spectrum of compound **4.**

40
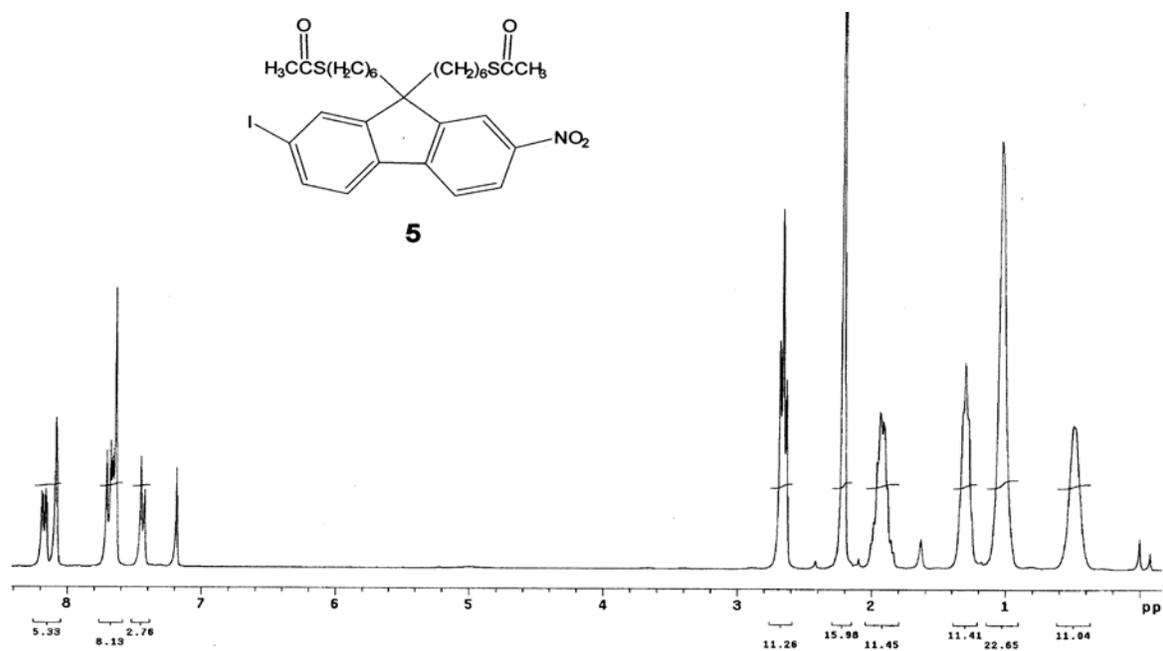
Figure 18. ^{1}H NMR spectrum of compound **5.**
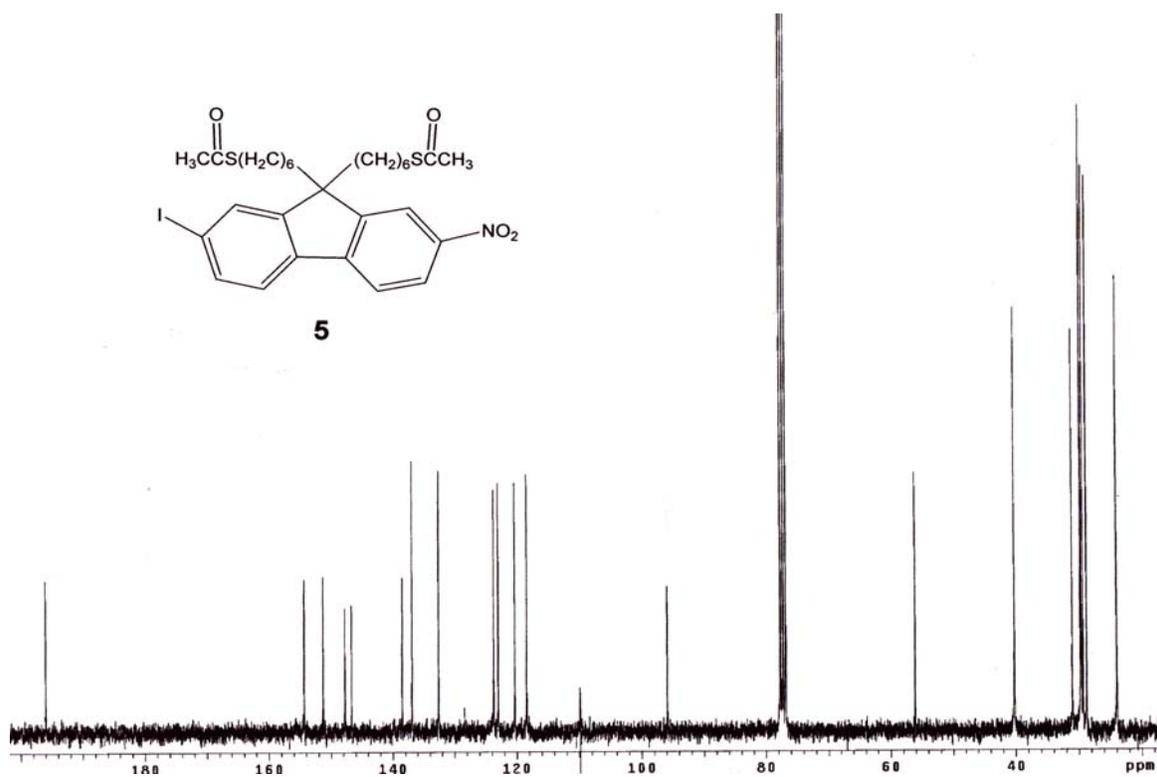
Figure 19. ^{13}C NMR spectrum of compound **5.**
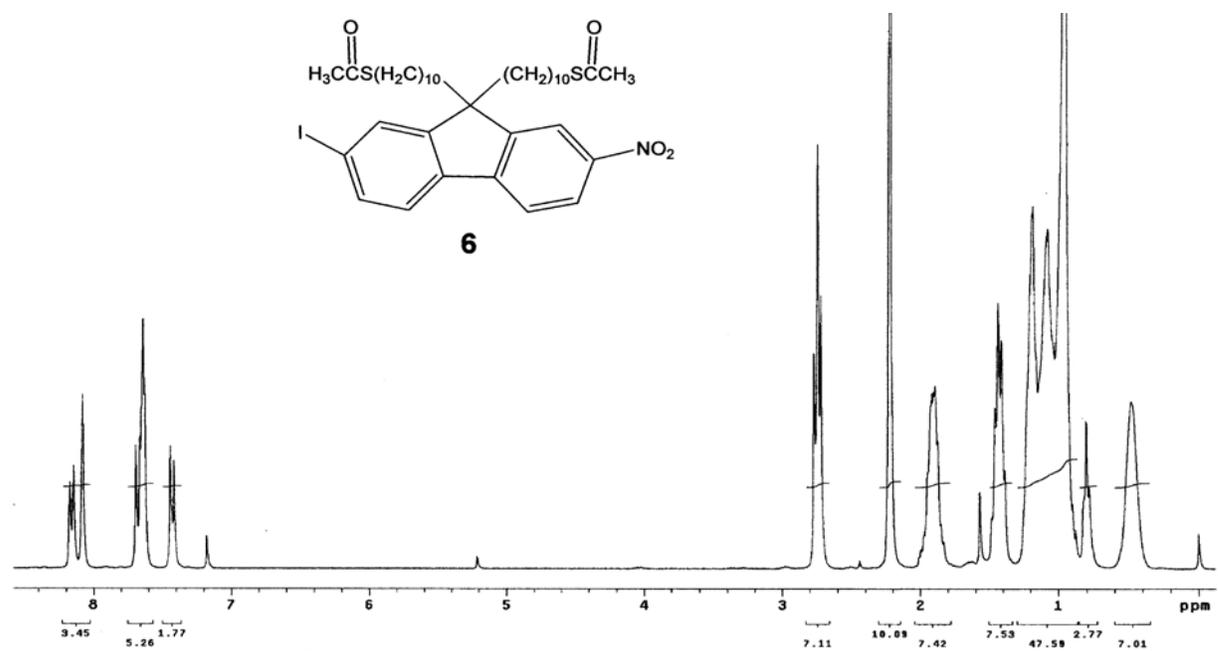
Figure 20. ^{1}H NMR spectrum of compound **6.**
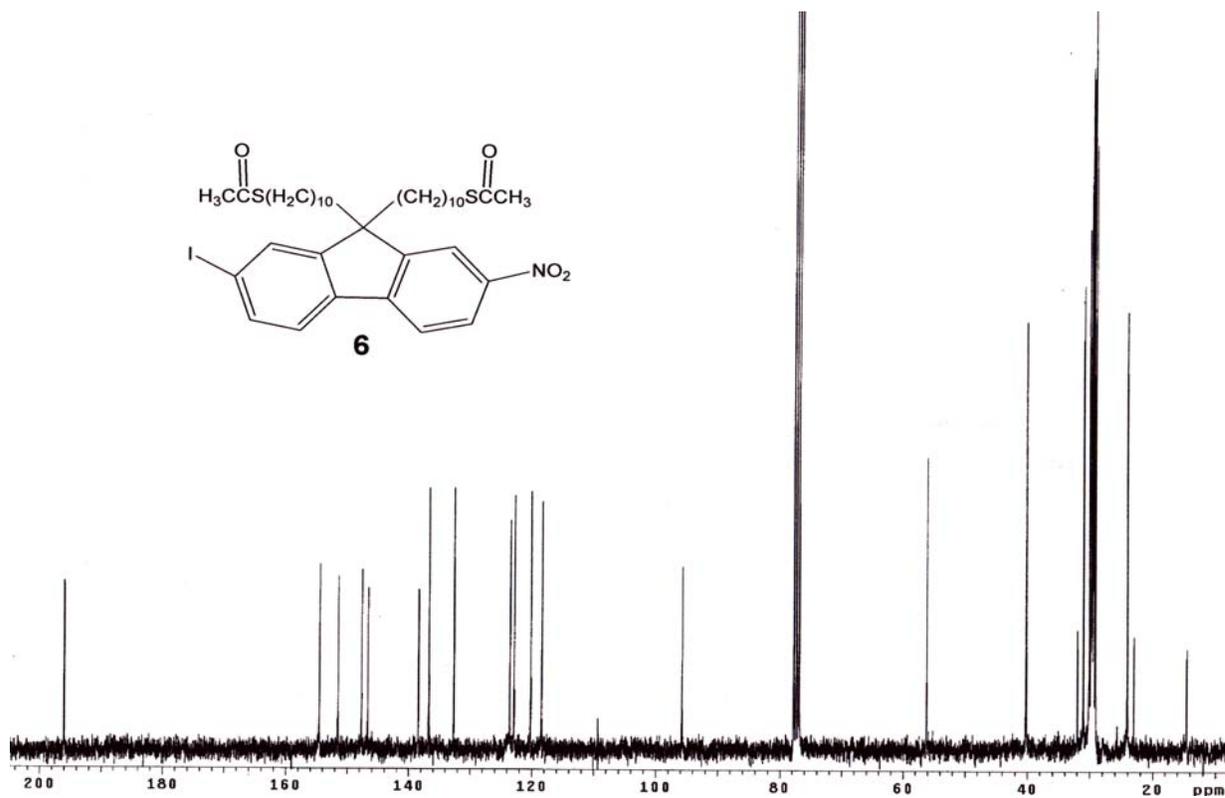
Figure 21. ^{13}C NMR spectrum of compound **6.**

42
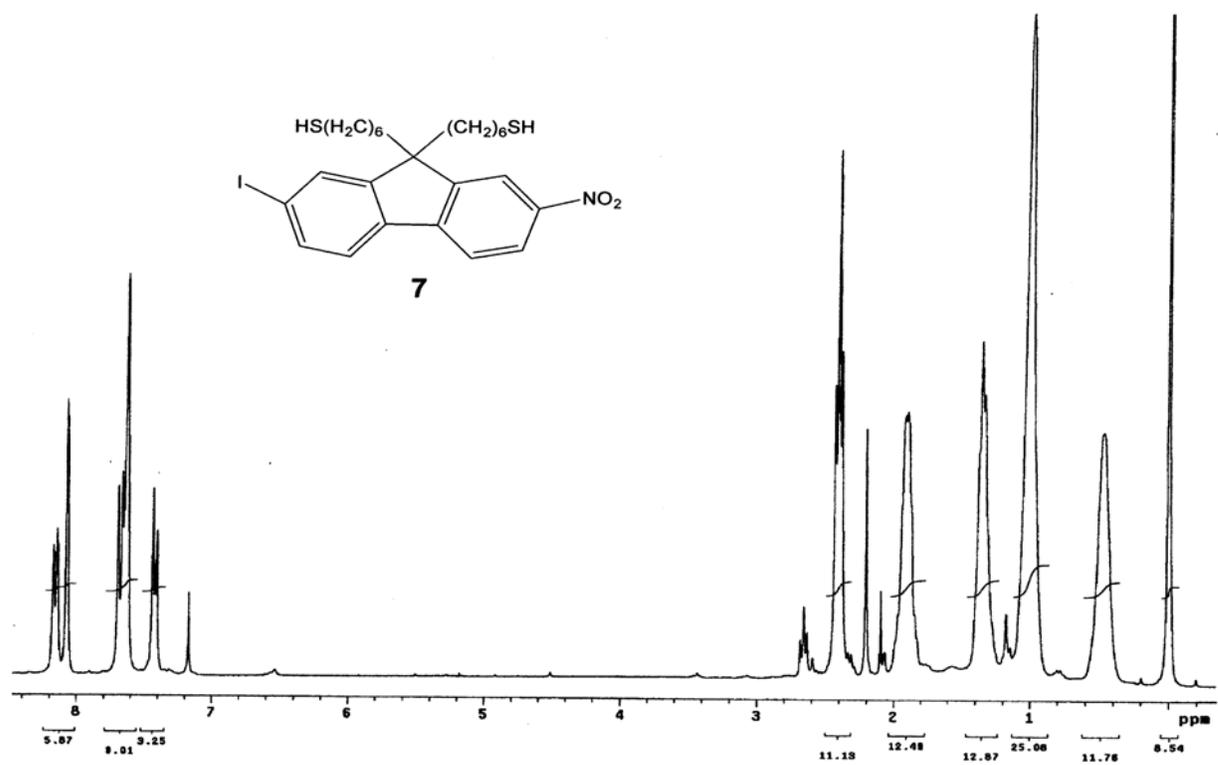
Figure 22. ^{1}H NMR spectrum of compound **7.**
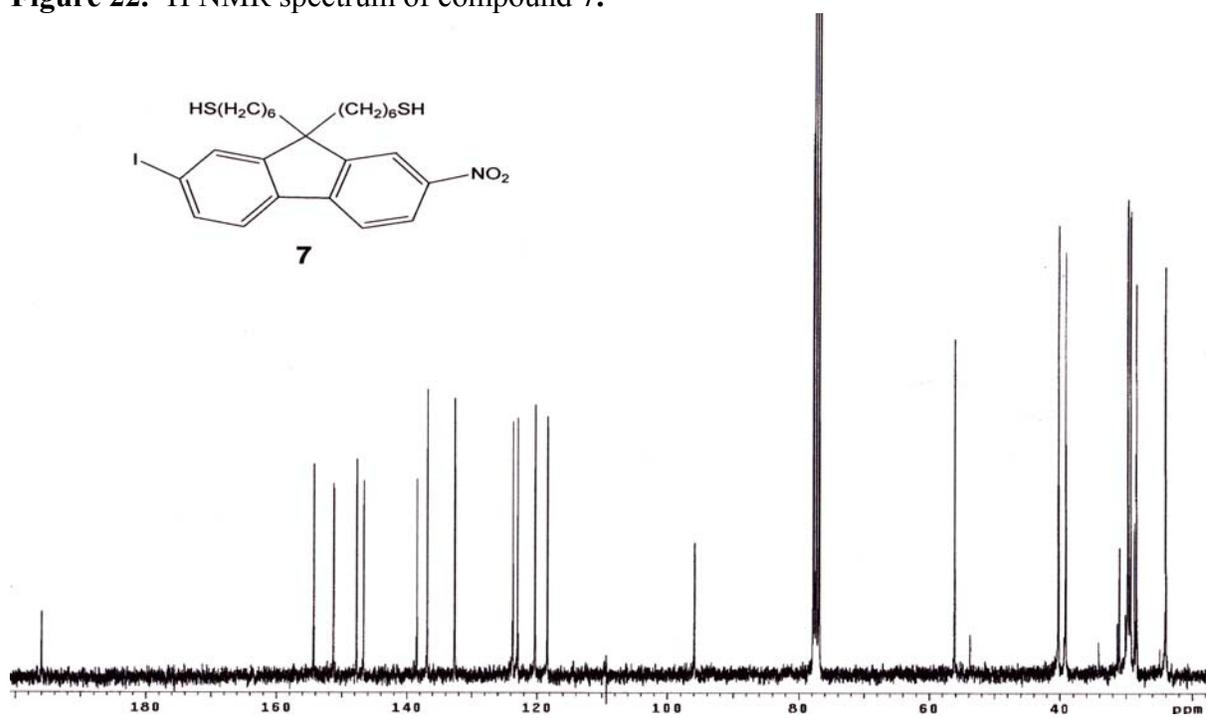
Figure 23. ^{13}C NMR spectrum of compound **7.**

43
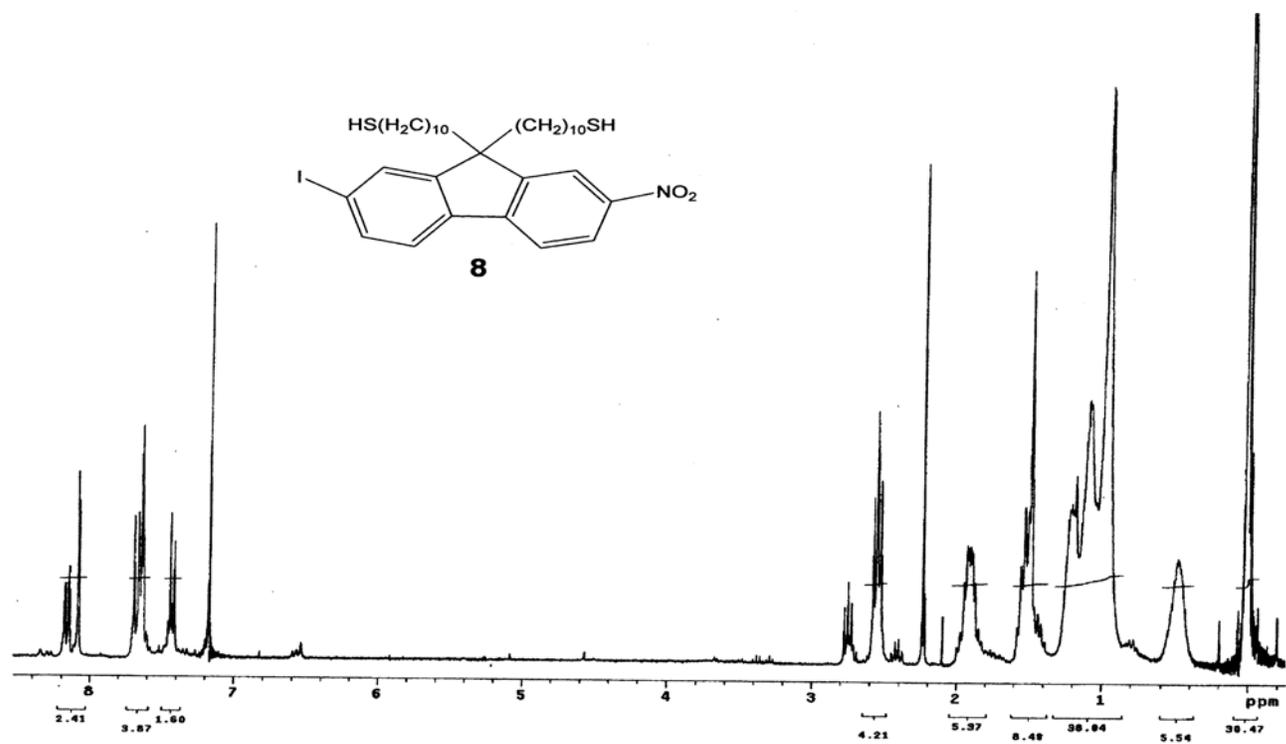
Figure 24. ^{1}H NMR spectrum of compound **8.**
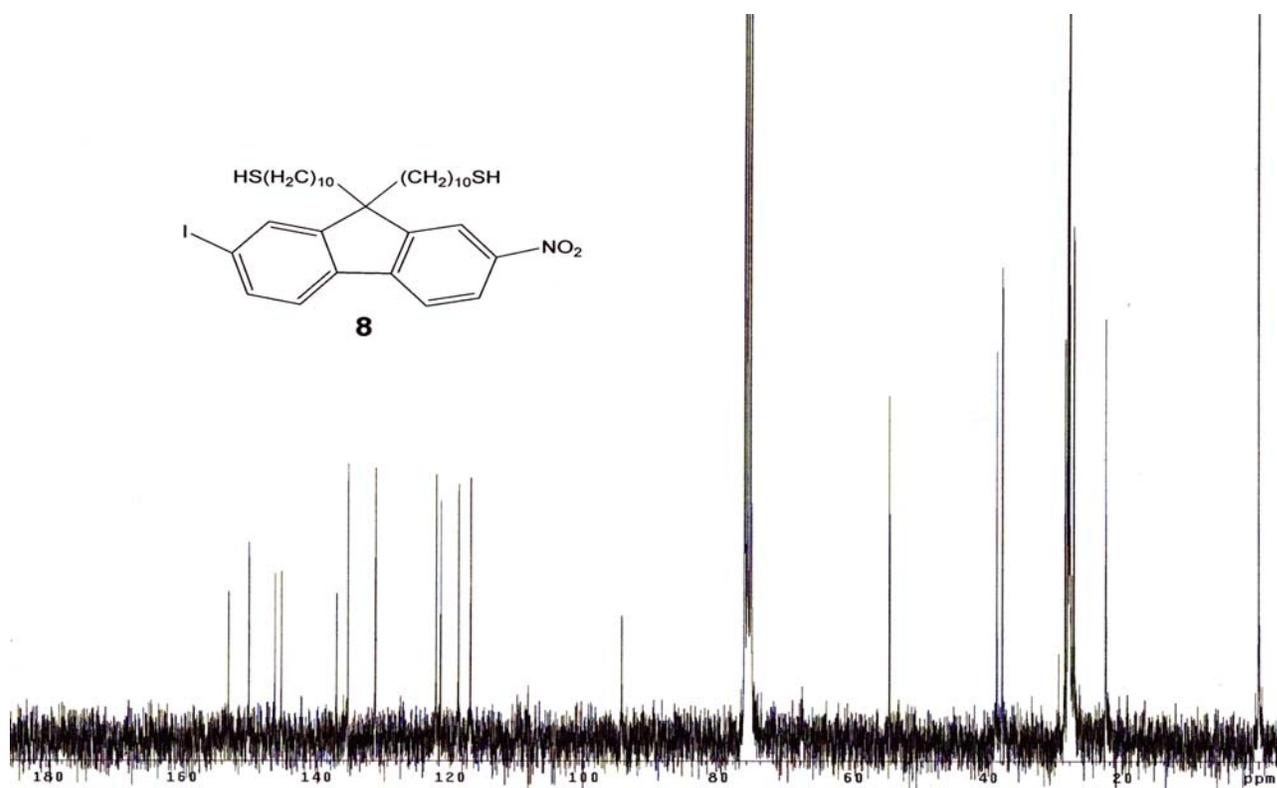
Figure 25. ^{13}C NMR spectrum of compound **8.**

44

Figure 26. ^{1}H NMR spectrum of compound **9.**

Figure 27. ^{13}C NMR spectrum of compound **9.**
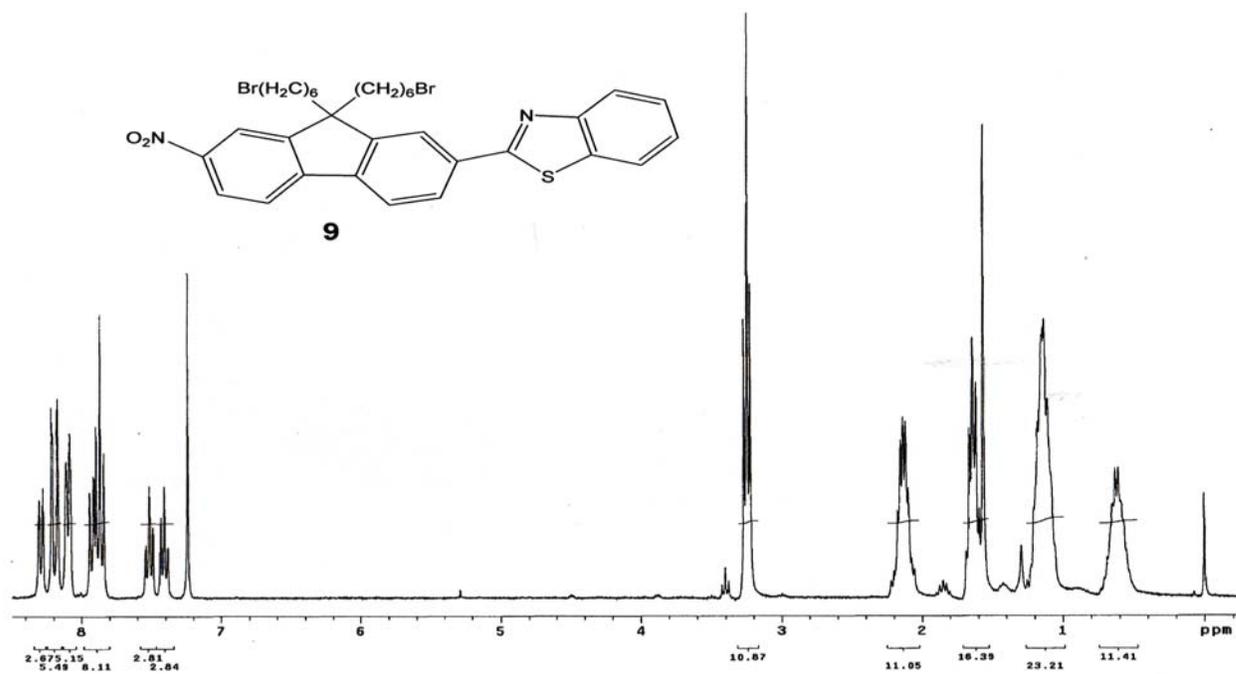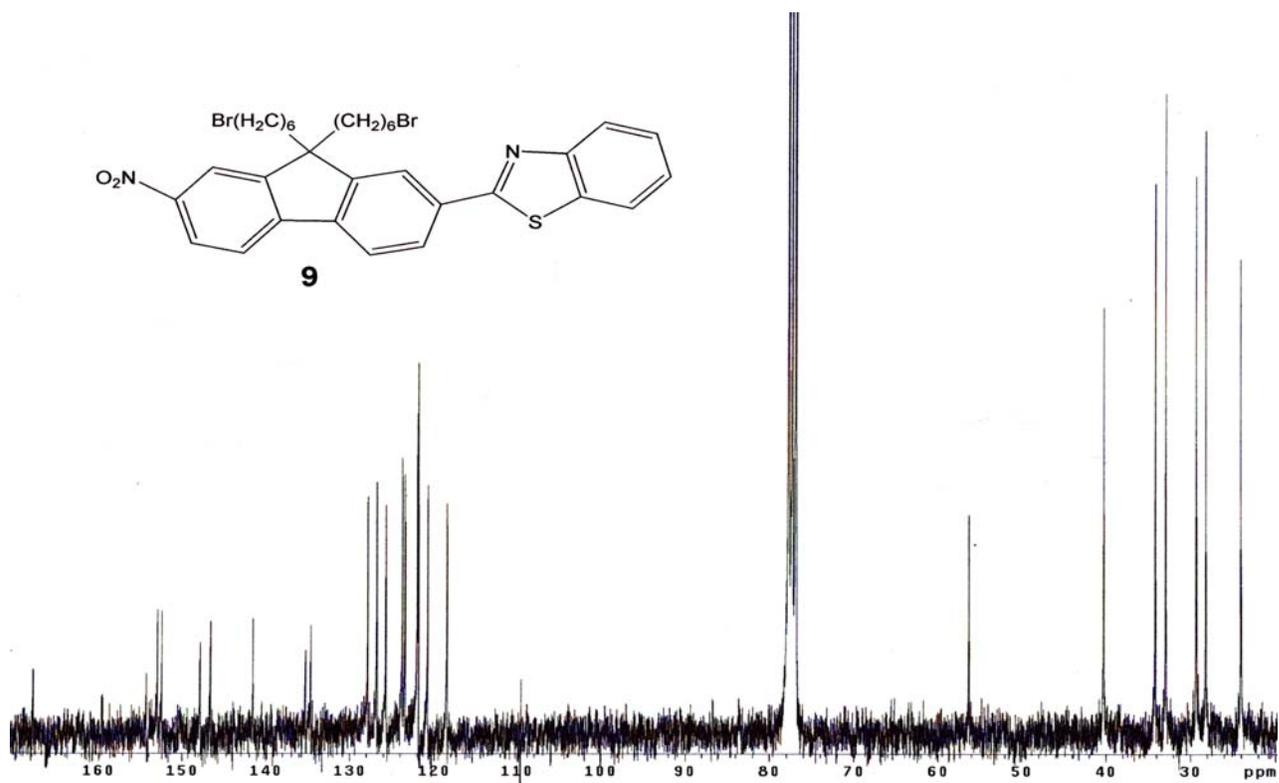
CHAPTER FOUR: CONCLUSIONS

A new synthetic methodology was developed to incorporate thioalkyl chains at the 9 position of the fluorene ring system possesing different types of electron donating and electron accepting groups. The work presented in this thesis represents the first step taken towards achieving our goal of establishing the foundation for applying the principles of RDE for enhanced singlet oxygen sensitization in two photon PDT by providing the synthetic means to generate functionalized materials. The synthesis is straightforward and is likely serve its purpose for incorporating thioalkyl chains to a series of fluorene based photosensitizers that our group has synthesized and characterized for their photochemical and photphysical properties.

Future work will mainly involve determining the appropriate conditions for attaching the thioalkylated photosensitizers to gold nanoparticles of different sizes in an efficient manner and prove that the functionalization has taken place. Accomplishment of this last step will open up a plethora of research avenues that nanoparticles can afford in applications like targeted drug delivery and bioimaging by making use of our group's dyes with high two photon absorption (2PA) cross-sections.

LIST OF REFERENCES

1. Lakowicz, J. R., Radiative decay engineering: biophysical and biomedical applications, *Anal. Biochem.* **2001**, *298*, 1-24.

2. Blackburn, G. F.; Shah, H. P.; Kenten, J. H.; Leland, J.; Link, J.; Peterman, J.; Powell, M. J.; Shah, A.; Talley, D. B.; Tyagi, S. K.; Wilkins, E.; Wu, T.G.; and Massey, R. J., Electrochemiluminescence detection for development of immunoassays and DNA probe assays for clinical diagnosis, *Clin. Chem.* **1991,** *37*, 1534-1539.

3. Van Orden, A.; Machara, N. P.; Goodwin, P. M.; Keller, R. A., Single-molecule identification in flowing sample streams by fluorescence burst size and intraburst fluorescence decay rate, *Anal. Chem.* **1998**, *70(7)*, 1444–1451.

4. The human genome, *Science* **2001**, *291*, 1177-1351.

5. Drexhage, K. H.; Interaction of light with monomolecular dye lasers, *Progress in Optics* **1974**, 161–232.

6. Amos, R. M.; and Barnes, W. L., Modification of the spontaneous emission rate of Eu^{3+} ions close to a thin metal mirror, *Phys. Rev. B* **1997**, *55*, 7249–7254.

7. Barnes, W. L., Fluorescence near interfaces: the role of photonic mode density. *J. Modern Optics* **1998**, *45*, 661–699.

8. Amos, R. M.; and Barnes, W. L., Modification of spontaneous emission lifetimes in the presence of corrugated metallic surfaces, *Phys. Rev. B* **1999**, *59*, 7708–7714.

9. Glass, A. M.; Liao, P. F.; Bergman, J. G.; and Olson, D. H., Interaction of metal particles with adsorbed dye molecules: Absorption and luminescence, *Optics Letts.* **1980**, *5*, 368–370.

10. Campion, A.; Gallo, A. R.; Harris, C. B.; Robota, H. J.; and Whitmore, P.M., Electronic energy transfer to metal surfaces: A test of classical image dipole theory at short distances, *Chem. Phys. Letts.* **1980**, *73*, 447–450.

11. Sokolov, K.; Chumanov, G.; and Cotton, T. M., Enhancement of molecular fluorescence near the surface of colloidal metal films, *Anal. Chem.* **1998**, *70*, 3898–3905.

12. Hayakawa, T.; Selvan, S. T.; and Nogami, M., Field enhancement effect of small Ag particles on the fluorescence from Eu^{3+}-doped SiO_2 glass **1999**, *74*, *Appl. Phys. Lett.*,1513–1515.

13. Selvan, S. T.; Hayakawa, T.; and Nogami, M., Remarkable influence of silver islands on the enhancement of fluorescence from Eu^{3+} ion-doped silica gels, *J. Phys. Chem. B* **1999**, *103*, 7064–7067.

14. Georghiou, S.; Nordlund, T. M.; and Saim, A. M., Picosecond fluorescence decay time measurements of nucleic acids at room temperature in aqueous solution, *Photochem. Photobiol.* **1985**, *41*, 209–212.

15. Daniel, E.; and Weber, G., Cooperative effects in binding by bovine serum albumin. I. the binding of 1-anilino-8-naphthalene-sulfonate. fluorimetric titrations. *Biochemistry*, **1966**, *5*,1893–1900.

16. Slavik, J., *Fluorescent probes in cellular and molecular biology*, CRC Press, Boca Raton, 1994.

17. Michaels, A. M.; Jiang, J.; and Brus, L., Ag nanocrystal junctions as the site for surface-enhanced Raman scattering of single rhodamine 6G molecules, *J. Phys. Chem. B.* **2000**, *104*, 11965–11971.

18. Freeman, R. G.; Grabar, K. C.; Allison, K. J.; Bright, R. M.; Davis, J. A.; Guthrie, A. P.; Hommer, M. B.; Jackson, M. A.; Smith, P. C.; Walter, D. G.; and Natan, M. J., Self-assembled metal colloid monolayers: An approach to SERS substrates, *Science* **1995**, *267*, 1629–1632.

19. Leitner, A.; Lippitsch, M. E.; Draxler, S; Riegler, M.; and Aussenegg, F. R., Fluorescence properties of dyes absorbed to silver islands, investigated by picosecond techniques, *Appl. Phys. B*, **1985** *36*,105–109.

20. Link, S.; and El-Sayed, M. A., Shape and size dependence of radiative, nonradiative and photothermal properties of gold nanocrystals, *Int. Rev. Phys. Chem.* **2000**, *19*, 409–453.

21. Kreibig, U.; and Vollmer, M., *Optical properties of metal clusters*, Springer Series in Materials Science, Springer Verlag, Berlin, 1995.

22. Philpott, M. R., Effect of surface plasmons on transitions in molecules, *J. Chem. Phys.* **1975**, *62*,1812–1817.

23. Chance, R. R.; Prock, A.; and Silbey, R., Molecular fluorescence and energy transfer near interfaces, *Adv. Chem. Phys.* **1978**, *37*, 1–65.

24. Gersten, J.; and Nitzan, A, Spectroscopic properties of molecules interacting with small dielectric particles, *J. Chem. Phys.* **1981**, *75*, 1139–1152.

25. Weitz, D. A.; Garoff, S.; Gersten, J. I.; and Nitzan, A., The enhancement of Raman scattering, resonance Raman scattering, and fluorescence from molecules absorbed on a rough silver surface, *J. Chem. Phys.* **1983**, *78*, 5324–5338.

26. Belfield, K. D.; Morales, A. R.; Kang, B. S.; Hales, J. M.; Hagan, D. J.; Van Stryland, E. W.; Chapela, V. M.; and Percino, J., Synthesis, characterization, and optical properties of new two-photon-absorbing fluorene derivatives**,** *Chem. Mater.* **2004**, *16(23)*, 4634-4641.

27. Belfield, K. D.; Bondar, M. V.; Przhonska, O. V.; and Schafer, K. J., Photochemical properties of (7-benzothiazol-2-yl-9, 9-didecylfluoren-2-yl) diphenylamine under one- and two- photon excitation, *J. Photochem. Photobiol. A: Chem.* **2004**, *162*, 569.

28. Belfield, K. D.; and Yao, S., Synthesis of two-photon absorbing unsymmetrical branched chromophores through direct tris(bromomethylation) of tluorene**,** *J. Org. Chem.* **2005**, *70(13)*, 5126-5132 .

29. Belfield, K. D. ; Corredor, C. C.; Morales, A. R. ; Dessources, M. A. ; Hernandez, F. E. "Synthesis and characterization of new fluorene-based singlet oxygen sensitizers" *Journal of Fluorescence* **2005**, in press. Belfield, K.D.; Bondar, M. V.; Przhonska, O. V. "Singlet oxygen quantum yield determination for a fluorene-based two-photon photosensitizer" *Journal of Fluorescence* **2005**, in press.

30. Alivisatos, A. P., Perspectives on the physical chemistry of semiconductor nanocrystals, *J. Phys. Chem.* **1996**, *100*, 13226.

31. Wang, Y., Nonlinear optical properties of nanometer-sized semiconductor clusters, *Acc. Chem. Res.* **1991**, *24*, 133.

32. Terrill, R. H.; Postlethwaite, T. A.; Chen, C. H.; Poon, C. D.; Terzis, A.; Chen, A. D.; Hutchinson, J. E.; Clark, M. R.; Wignall, G.; Londono, J. D.; Superfine, R.; Falvo, M.; Johnson, C. S.; Samulski, E. T.; and Murray, R. W., Monolayers in three dimensions; NMR, SAXS, thermal, and electron hopping studies of alkanethiol stabilized gold clusters, *J. Am. Chem. Soc.* **1995**, *117*, 12537-12548.

33. Templeton, A. C.; Hostetler, M. J.; Warmoth, E. K.; Chen, S. W.; Hartshorn, C. M.; Krishnamurthy, V. M.; Forbes, M. D. E.; Murray, R. W., Gateway reactions to diverse, polyfunctional monolayer-protected gold clusters, *J. Am. Chem. Soc.* **1998**, *120*, 4845-4849.

34. Chen, S. W.; Murray, R. W., Arenethiolate monolayer-protected gold clusters, *Langmuir* **1999**, *15*, 682-689.

35. Aguila, A.; Murray, R. W.,Monolayer-protected clusters with fluorescent dansyl ligands, *Langmuir* **2000**, *16*, 5949-5954.

36. Chen, S. W.; Templeton, A. C.; Murray, R. W., Monolayer-protected cluster growth dynamics , *Langmuir* **2000**, *16*, 3543-3548.

37. Badia, A.; Cuccia, L.; Demers, L.; Morin, F.; Lennox, R. B., Structure and dynamics in alkanethiolate monolayers self-assembled on gold nanoparticles: A DSC, FT-IR, and Deuterium NMR Study, *J. Am. Chem. Soc.* **1997**, *2*, 42-50.

38. Gu, T.; Ye, T.; Simon, J. D.; Whitesell, J. K.; and Fox, M. A., Subpicosecond transient dynamics in gold nanoparticles encapsulataed by a fluorophore-terminated monolayer, *J. Phys. Chem. B.* **2003**, *107*, 1765-1771.

39. Gu, T.; Whitesell, J. K.; and Fox, M. A., Energy transfer from a surface-bound arene to the gold core in ω-fluorenyl-alkane-1-thiolate monolayer-protected gold clusters, *Chem. Mater.* **2003**, *15*, 1358-1366

40. Kuhn, W. E. *Organic synthesis, Coll. Vol. 2*; Blatt, A. H., Ed.; Wiley: New York, 1943, pp. 447.

41. Markevka, V. C.; Ebner, N. A.; Sehon, R. D.; Hanna, P. E., Mechanism-based inactivation of N-arylhydroxamic acid N, O-acyltransferase by 7-substituted-N-hydroxy-2-acetamidofluorenes, *J. Med. Chem.* **1985**, *28*, 18.

42. Suh, Y. S.; Ko, S. W.; Jung, B. J.; Shim, H. K., Synthesis and electroluminescent properties of cyclohexyl-substituted ployfluorenes, *Opt. Mater.* **2002**, *21*, 109.

43. Zheng, T. C.; Burkart, M.; Richardson, D. E., A general and mild synthesis of thioesters and thiols from halides, *Tet. Lett*. **1999**, *40*, 603.